Article

Cell

A Human Interactome in Three Quantitative Dimensions Organized by Stoichiometries and Abundances

Graphical Abstract

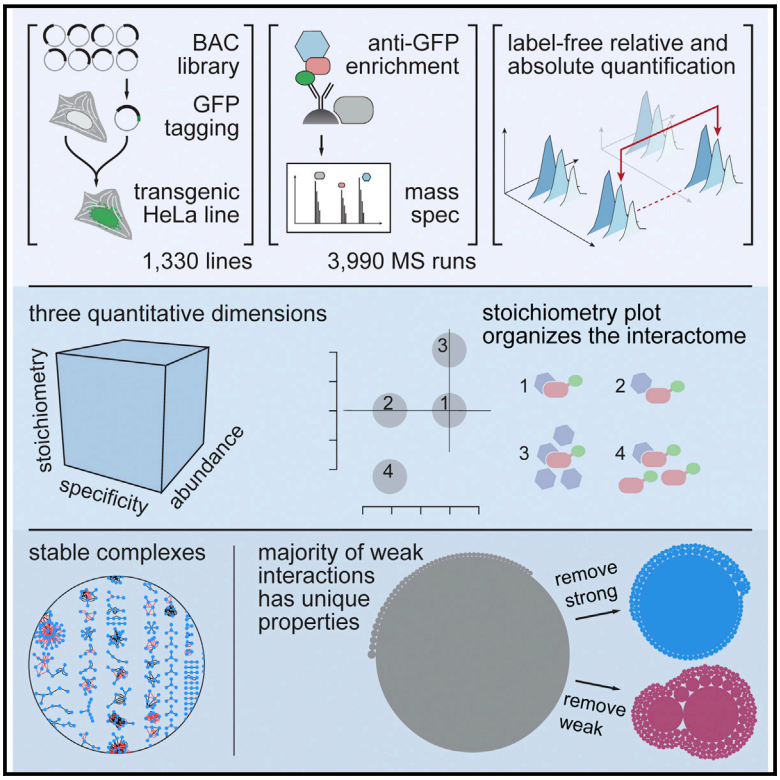

Highlights

- Human interactome dataset connecting 5,400 proteins with 28,500 interactions
- Three quantitative dimensions measure specificities, stoichiometries, and abundances
- Stable complexes are rare but stand out by a signature of balanced stoichiometries
- Weak interactions dominate the network and have critical topological properties

Authors

Marco Y. Hein, Nina C. Hubner, Ina Poser, ..., Frank Buchholz, Anthony A. Hyman, Matthias Mann

Correspondence

hyman@mpi-cbg.de (A.A.H.), mmann@biochem.mpg.de (M.M.)

In Brief

Weak interactions shape the cellular protein interaction network as determined from proteomic measures of cellular interaction specificities, the strength of those interactions, and the cellular copy numbers of the proteins involved.

Hein et al., 2015, Cell *163*, 712–723
October 22, 2015 ©2015 Elsevier Inc.
http://dx.doi.org/10.1016/j.cell.2015.09.053

Cell

Article

A Human Interactome in Three Quantitative Dimensions Organized by Stoichiometries and Abundances

Marco Y. Hein,[1,6,8] Nina C. Hubner,[1,6,9] Ina Poser,[2] Jürgen Cox,[1] Nagarjuna Nagaraj,[1] Yusuke Toyoda,[2,10] Igor A. Gak,[3] Ina Weisswange,[4,5] Jörg Mansfeld,[3] Frank Buchholz,[2,4] Anthony A. Hyman,[2,7,*] and Matthias Mann[1,7,*]

[1]Max Planck Institute of Biochemistry, 82152 Martinsried, Germany
[2]Max Planck Institute of Molecular Cell Biology and Genetics, 01307 Dresden, Germany
[3]Cell Cycle, Biotechnology Center, TU Dresden, 01307 Dresden, Germany
[4]Medical Systems Biology, UCC, Medical Faculty Carl Gustav Carus, TU Dresden, 01307 Dresden, Germany
[5]Eupheria Biotech GmbH, 01307 Dresden, Germany
[6]Co-first author
[7]Co-senior author
[8]Present address: Howard Hughes Medical Institute, University of California San Francisco, San Francisco, CA 94143, USA
[9]Present address: Department of Molecular Biology, Faculty of Science, Radboud Institute for Molecular Life Sciences, Radboud University Nijmegen, Nijmegen 6525 GA, the Netherlands
[10]Present address: Institute of Life Science, Kurume University, Kurume, Fukuoka 839-0864, Japan
*Correspondence: hyman@mpi-cbg.de (A.A.H.), mmann@biochem.mpg.de (M.M.)
http://dx.doi.org/10.1016/j.cell.2015.09.053

SUMMARY

The organization of a cell emerges from the interactions in protein networks. The interactome is critically dependent on the strengths of interactions and the cellular abundances of the connected proteins, both of which span orders of magnitude. However, these aspects have not yet been analyzed globally. Here, we have generated a library of HeLa cell lines expressing 1,125 GFP-tagged proteins under near-endogenous control, which we used as input for a next-generation interaction survey. Using quantitative proteomics, we detect specific interactions, estimate interaction stoichiometries, and measure cellular abundances of interacting proteins. These three quantitative dimensions reveal that the protein network is dominated by weak, substoichiometric interactions that play a pivotal role in defining network topology. The minority of stable complexes can be identified by their unique stoichiometry signature. This study provides a rich interaction dataset connecting thousands of proteins and introduces a framework for quantitative network analysis.

INTRODUCTION

Proteins are central protagonists of life at the molecular level. They interact for structural, regulatory, and catalytic purposes, forming macromolecular structures as well as stable or transient multi-protein complexes. Accordingly, protein interactions vary greatly in their biophysical properties, while protein abundances range from a few to millions of copies per cell. The interactome is therefore the product of two factors: binary affinities between protein interfaces (Rual et al., 2005; Stelzl et al., 2005; Rolland et al., 2014) and the cellular proteome, which itself is characterized by subcellular localization, post-translational modifications and protein concentrations (Hein et al., 2013; Mann et al., 2013).

Mapping the protein interactome landscape has been a long-standing goal of modern biology and a variety of methods have been developed to this end (Seebacher and Gavin, 2011). Affinity purification followed by mass spectrometry (AP-MS) can in principle determine the members of protein complexes in their cellular context in an unbiased manner (Gingras et al., 2007) and has enabled large-scale protein interaction studies of several model organisms, including human cells (Ewing et al., 2007; Malovannaya et al., 2011). Nanoscale liquid chromatography (LC) coupled to sensitive and fast mass spectrometers has boosted interaction proteomics technology in recent years, increasing coverage and minimizing false negative rates. It has also enabled a paradigm shift from identification to quantification of interacting proteins (Bantscheff et al., 2012). Quantitative approaches permit the use of mild immunoprecipitation (IP) protocols and allow specific binders to stand out by their quantitative signature even from very large backgrounds of unspecific proteins (Mellacheruvu et al., 2013; Keilhauer et al., 2015). Additionally, MS-based proteomics is now able to characterize entire cellular proteomes with increasingly complete coverage (Beck et al., 2011; Mann et al., 2013), providing abundances and copy-number estimates of the expressed proteins. This should now allow studying the quantitative interactome as a function of the underlying proteome. To generate model systems that closely recapitulate in vivo conditions, we have previously developed bacterial artificial chromosome (BAC) transgeneomics: GFP-tagged proteins are expressed in mammalian cell lines from BAC transgenes with near-endogenous expression patterns from human or orthologous mouse loci (Poser et al., 2008). GFP-based tags are dual-purpose in that they can be used for both imaging and as affinity handle. Combining these

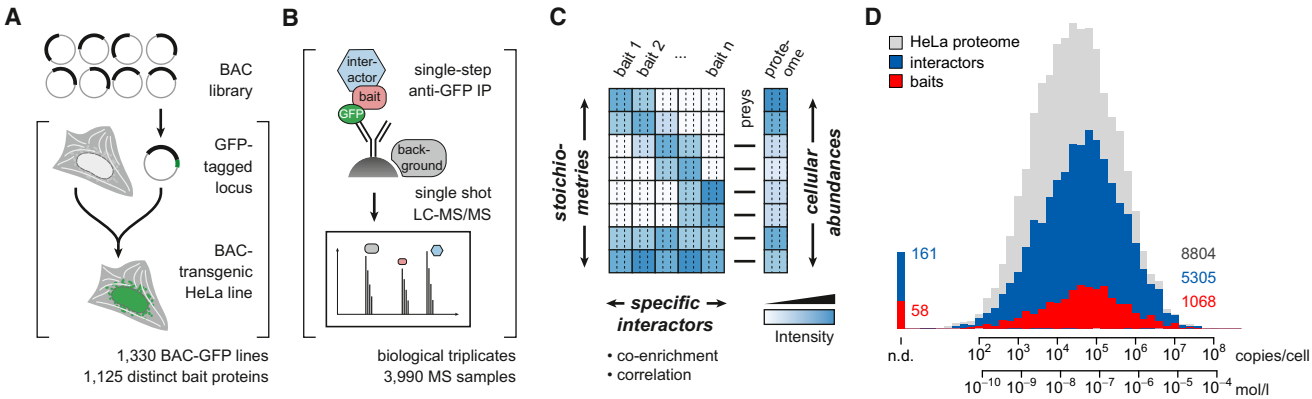

Figure 1. Quantitative BAC-GFP Interactomics

(A) BAC recombineering workflow for generating transgenic HeLa lines.

(B) Single-step affinity-purification, single-run liquid chromatography-tandem mass spectrometry (LC-MS/MS) workflow.

(C) Schematic protein quantification matrices in interactome and proteome samples with three dimensions of quantification.

(D) Proteome coverage and abundance distribution of the bait proteins and their interactors.

See also Tables S1, S2, and S3.

cell lines with the quantitative proteomics workflow resulted in a versatile and highly specific method that we termed quantitative BAC-GFP interactomics (QUBIC) (Hubner et al., 2010).

Here, we applied QUBIC in a proteome-wide manner, using 1,125 bait proteins to assemble a large-scale map of the human interactome. We characterize individual interactions in three quantitative dimensions that address statistical significance, interaction stoichiometry, and cellular abundances of interactors. This concept provides a unique perspective on the interactome, enabling the discovery and characterization of stable and transient protein complexes, guiding their functional interpretation and shedding light on the topological architecture of the entire network.

RESULTS

Quantitative BAC-GFP Interactomics

Collections of strains or cell lines expressing tagged proteins are indispensable tools for many systems biology approaches (Huh et al., 2003). Expressing GFP-tagged proteins from engineered BAC transgenes maintains the endogenous promoters, intron-exon-structures and regulatory elements, ensuring near-endogenous expression levels and patterns (Poser et al., 2008) (Figure S1A). We have previously used this system to study chromosome segregation and the function of motor proteins (Hutchins et al., 2010; Maliga et al., 2013). To map the protein interactome globally, we generated a resource of 1,330 stable BAC-GFP HeLa cell lines (Figure 1A; Table S1). Mouse BACs are excellent surrogates for their human orthologs and offer additional options, such as resistance to RNAi against their endogenous counterparts, streamlining functional studies of the tagged proteins (Kittler et al., 2005). In 615 cell lines, we used mouse BACs with a median sequence identity of 94% with their respective orthologs (Figure S1B). Overall, our collection encompasses 1,125 distinct bait proteins across all protein classes (Figures S1C–S1E), some present as C- and N-terminally tagged versions, or as mouse and human sequences (not counted as distinct).

We performed QUBIC in three biological replicate experiments, resulting in 3,990 LC-MS runs recorded on an Orbitrap mass spectrometer, taking about a year of net measuring time (Figure 1B). To define specific interactors, we employed MaxLFQ, the label-free quantification (LFQ) module of the MaxQuant software (Cox and Mann, 2008; Cox et al., 2014). Bait proteins and their interactors are characterized by quantitative co-enrichment compared to their intensity profiles across many samples (Figures 1B and 1C), and we used generic statistical testing to determine significantly enriched cases (Keilhauer et al., 2015). To set thresholds for accepting a given candidate as an interactor, we developed an entirely data-driven, false discovery rate (FDR)-controlled approach that harnesses the absence of "negative" interactions and the concomitant asymmetry of the outlier population (Figures S1F and S1G). This approach does not rely on reference datasets or prior knowledge for training, but nonetheless validates favorably against gold standards (Figures S1I–S1K).

In addition to local co-enrichment, we found the intensity profiles of interacting proteins to be closely correlated globally (Supplemental Experimental Procedures). Profile correlations alone can indicate protein interactions when proteome samples are subjected to extensive native fractionation (Havugimana et al., 2012; Kristensen et al., 2012). Here, we use them as additional classifiers (Keilhauer et al., 2015) and the combination of enrichment FDRs and profile correlation coefficients defines the confidence class of each interaction (Figure S1H).

Overall, using the information in this first dimension of proteomic quantification, our analysis resulted in 28,504 unique and statistically significant interactions involving 5,462 distinct proteins (Table S2).

Interaction Stoichiometries and Protein Abundances

A second dimension of quantification can in principle be applied to determine the stoichiometries of proteins within complexes.

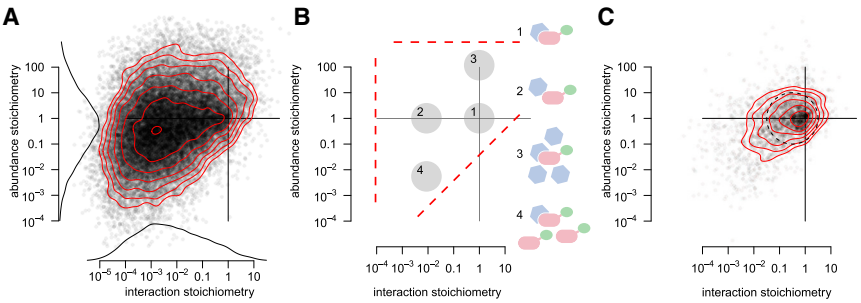

Figure 2. The Stoichiometry Plot

(A) Overlay of all interaction and abundance stoichiometry data for all interactions.

(B) The characteristic triangular shape is a consequence of the dynamic range limits in the interactome (left border), in the proteome (top border) and the stoichiometry limit imposed by the relative cellular protein abundances (diagonal). Schematic interaction scenarios: (1) equal cellular abundance, stable interaction; (2) equal cellular abundance, weak interaction; (3) stable interaction with greater cellular abundance of the prey; and (4) reciprocal case: quantitative recovery of a stably bound, less abundant prey.

(C) Stoichiometry plot of interactions between proteins annotated as CORUM complex members. The area of highest density can be approximated by a circle containing 58% of CORUM interactions.

See also Data S1.

These can be computationally extracted from label-free affinity purification data with accuracies reaching those of methods using isotopically labeled reference standards (Wepf et al., 2009; Smits et al., 2012). If a protein complex contained one copy of each subunit, one might expect them to be retrieved in equimolar amounts after immunoprecipitation (IP). However, in practice, measured stoichiometries between preys and baits span orders of magnitude (Collins et al., 2013; Hauri et al., 2013). This is because the observed stoichiometries depend on more than the initial composition of the individual complexes in the cell. For instance, limited kinetic and thermodynamic stability can result in substoichiometric recovery. Proteins may also reside in different alternative molecular assemblies with fractions of their total cellular pools. Hence, we hypothesized that globally, interaction stoichiometries might reflect the stability of a given protein-protein interaction and depend on the extent that interactors are engaged with each other. The cellular abundance of an interactor can be limiting for how much is recoverable after immunoprecipitation (IP), setting a lower bound for the interaction stoichiometry. We therefore reasoned that cellular copy numbers would provide a crucial third quantitative dimension.

For each pair of interacting proteins, we first quantified their stoichiometry in the immunoprecipitates using a sophisticated label-free strategy for absolute protein quantification (Supplemental Experimental Procedures). To determine the precision of our method, we systematically compared interaction stoichiometries from experiments where the same bait proteins were tagged on different termini, representing entirely separate experiments (Figures S2A and S2E). Stoichiometries showed high correlation, precision within a factor of three, and no systematic bias for a given terminus. This confirmed that our approach robustly delivers interaction stoichiometries in high throughput; however, these may not always be sufficiently accurate to reliably specify copy numbers of each subunit, even for stable complexes. We repeated the analysis for cases where either the mouse or human ortholog of a protein was used as bait, demonstrating the same level of reliability and no species bias (Figures S2B–S2D). This highlights the extraordinary degree of conservation of protein function in evolutionary time (Kachroo et al., 2015) and suggests that our human-centric dataset is representative not only of the human but other mammalian species.

To add a third dimension of proteomic quantification, we next performed a whole proteome quantification experiment on the parental HeLa cell line that all our BAC-transgenic lines are derived from, to a depth of about 9,000 proteins. To estimate cellular protein abundances, we applied our label-free approach and scaled the values to copies per cell using the "proteomic ruler" concept (Wiśniewski et al., 2014) (Supplemental Experimental Procedures). The proteome dataset provided cellular copy numbers for 5,305 proteins of the interactome dataset, covering 97% of all interactors (Figure 1D). The abundances of interacting proteins closely follow the distribution of bait abundances, covering the entire dynamic range of the proteome. This demonstrates that our BAC-based system recapitulates the in vivo situation, enabling us to probe the interactome as a function of the endogenous cellular proteome.

Quantifying the Interactome in Two Additional Dimensions

Having established a set of specific interactions with the first dimension of quantification, we next combined our second and third dimension of quantification, namely the interaction stoichiometries and relative cellular abundances of interactors. A plot of the stoichiometry landscape for each bait protein is a powerful tool to organize its interactome, because each region reflects a different scenario (Figures 2A and 2B): stable, one-to-one, and fully recovered complexes in which the partners have equal cellular abundance appear around the origin of the plot (case 1 in Figure 2B). Superstoichiometry, the recovery of more prey than bait, is only expected for stable complexes containing more prey than bait copies and indeed we find few of these. If interactions are weak and complexes dissociate partially during IP, or if interactions involve only part of the bait pool, interactors are recovered at substoichiometric levels (case 2), reflecting lower occupancy of interaction interfaces of the bait. A vast predominance of sub- over superstoichiometry confirms our initial hypothesis that stability and occupancy are the main determinants for most interactions.

We observed many cases of stable interactors (~1:1 interaction stoichiometry) that involved a more abundant prey (case 3), such as the interaction of the abundant GTP-binding protein RAN with its guanine-nucleotide releasing factor RCC1 or that of α-tubulin with the NEK9 kinase (see Table S2). The reciprocal

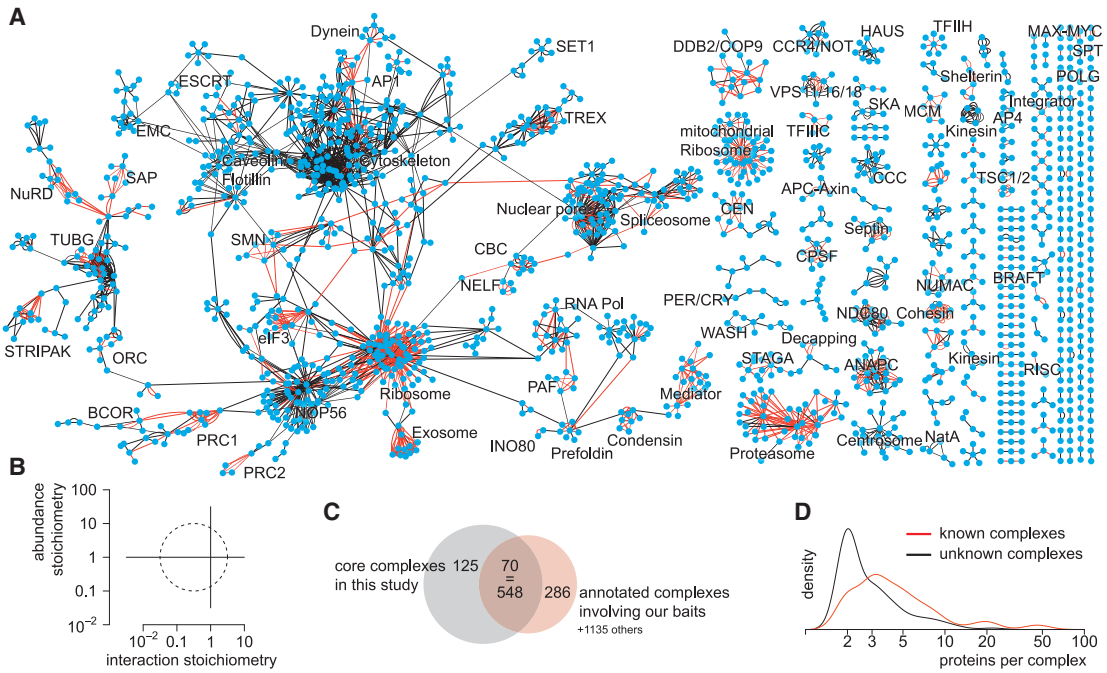

Figure 3. The Core-Complex Network

(A) Sub-networks of interactions matching the CORUM-characteristic core stoichiometry signature. Red edges are known interactions annotated in UniProt or CORUM.

(B) Graphical definition of the core stoichiometry signature. Center: −0.5, 0; radius: 1 ($\log_{10}$ units).

(C) Quantification of the CORUM overlap. A total of 125 isolated networks remain unannotated; 70 networks are annotated with 548 partially redundant CORUM terms; 286 terms assigned to our baits were not shared by any interactor.

(D) Size distribution of annotated versus unannotated networks.

See also Figure S3.

interaction stoichiometry readouts are necessarily smaller than one, because any higher abundant bait can maximally recover the entire pool of its lower abundant prey (case 4). (Note that this would be the default case for overexpressed baits.) We retrieved substoichiometric interactions over an estimated five orders of magnitude; for example, NEK9 was recovered at $6 \times 10^{-6} \times$ the amount of α-tubulin. The proteome-interactome relationship requires that interactors can only be recovered to the extent permitted by their abundance and translates into a diagonal cut-off in the plot, which results in a characteristic triangular shape of the "cloud" of interactions (Figure 2A).

Approximately 10% of our interactions connected members of well-characterized complexes annotated in the CORUM database (Ruepp et al., 2010). They populate a confined area characterized by a signature of balanced stoichiometries (case 1 in Figure 2B). Thus the prototypical case of a stable protein complex as typically described in the literature mostly consists of proteins of equal cellular abundances that are all constitutively bound to each other.

Extrapolating from the signature of known complexes, we reasoned that deduction of similar complexes should be possible solely from the stoichiometry signature of individual baits as opposed to analysis of the entire network (Collins et al., 2007; Hart et al., 2007). We filtered our data for those featuring the core stoichiometry signature (Figure 3B), yielding a larger cluster connecting several molecular assemblies such as major cytoskeletal proteins, the nuclear pore complex and the ribosome as well as 194 isolated putative core complexes (Figure 3A). These recapitulated the majority of CORUM-annotated complexes that involve our bait proteins (Figure 3C). We confirmed the known tendency of large complexes to be well annotated (Havugimana et al., 2012), while smaller assemblies lacked previous description (Figure 3D). The largest of our 125 networks with no database annotation at the time is the recently discovered COMMD/CCDC22/CCDC93 (CCC) complex (Phillips-Krawczak et al., 2015).

The stoichiometry plot offers a unique opportunity for comparing the overlap of our dataset with published data (Figures S3A–S3C). For instance, the intersection with a recent co-fractionation interactome study (Havugimana et al., 2012) closely recapitulated the core-complex signature, with 26% of our core-interactions overlapping with that study. This indicates that the co-fractionation methodology offers an attractive short-cut to finding stable, obligate core complexes. Conversely, the overlap with iRefWeb, a portal of consolidated protein interactions from different sources (Turner et al., 2010), reached much further into the substoichiometric region, beyond stable complexes, but still only covered 16% of our dataset. Finally, the overlap with recent large-scale yeast-two-hybrid data (Rolland et al., 2014) was low (0.4%) and mostly limited to cases characterized by quantitative

prey recovery to the extent permitted by cellular abundance. Moreover, the stoichiometry plot quantitatively confirmed the intuitive notion that high-stoichiometry interactions are easier to detect as they are enriched in the 1% FDR compared to the 5% FDR cohort (Figures S3D and S3E). This is also reflected in the overlap of gene ontology (GO) annotations in pairs of interacting proteins (Figure S3F).

Interactions Explain Phenotypes and Genetic Associations

Our dataset provides an extensive resource that can be mined for new or poorly characterized protein interactions. For instance, among the interactors of SUCO, one other protein, TAPT1, stood out by its core stoichiometry signature, suggesting a novel, stable complex consisting of these two low abundant integral membrane proteins of the ER (Figures 4A, 4B, and S4A–S4C). Mutants of their murine orthologs exhibit severe defects during skeletal development: Truncation of TAPT1 causes transformations in the axial skeleton and perinatal lethality (Howell et al., 2007), whereas loss of the SUN domain-containing ossification factor SUCO (also known as OPT) impairs postnatal bone formation, causing fractures and neonatal death (Sohaskey et al., 2010). The latter study linked the phenotype to impaired rough ER expansion and consequent failure of osteoblasts to secrete collagen required for bone formation. Knockdown of human SUCO increased the cells' resistance against ricin, whose toxicity depends on endocytosis and retrograde trafficking to the ER (Bassik et al., 2013). Similarly, the yeast ortholog of TAPT1, EMP65 (YER140W), is involved in protein folding in the ER and shows buffering genetic and physical interactions with the SUN domain protein SLP1 (YOR154W) (Jonikas et al., 2009; Friederichs et al., 2012). We used our interaction methodology on GFP-tagged strains to confirm this complex (Figures S4D and S4E). Similarly, we validated the reciprocal interaction in the mammalian system using TAPT1 as bait (Figure S4B). Together, our findings establish TAPT1–SUCO as the higher eukaryote ortholog of SLP1-EMP65: a low abundant ER membrane complex that is required for normal skeletal development.

Going beyond stable complexes, we discovered an interaction between the anaphase promoting complex or cyclosome (APC/C) and the uncharacterized protein KIAA1430. The stoichiometry plot indicated that KIAA1430 is of lower cellular abundance and is not an obligate member of the APC/C, as the partners were recovered substoichiometrically at ~1% of the respective baits in reciprocal experiments (Figures 4C and 4D).

To independently test whether KIAA1430 was indeed a transient interactor of the APC/C, we performed a purify-after-mixing (PAM)-SILAC experiment (Wang and Huang, 2008) (Figures 4E and 4F; Supplemental Experimental Procedures). We mixed differentially SILAC-labeled lysates from tagged and control cell lines before the affinity step. Subsequently measured SILAC ratios are indicative of the stability of the interaction, because transient interactors exchange dynamically with unbound counterparts, shifting their ratio toward unity, whereas stable interactors maintain their label ratio. Our results confirmed that only known subunits of the APC/C are stably bound to the core subunit CDC23. Consistently, only some of them were recovered when assayed for binding to KIAA1430 and with ratios indicating a high degree of dynamic exchange. Next, we tested whether KIAA1430 is a substrate of the APC/C by monitoring its levels during mitosis and early G1 phase. Unlike known substrates, KIAA1430 levels remained stable (Figure S4F).

In interphase, a fraction of GFP-tagged KIAA1430 localized to the centrosomes, in particular the centrioles, and was largely excluded from the nucleus (Figures 4G, 4H, S4G, and S4H), while the APC/C is known to be predominantly nuclear (Kraft et al., 2003; Hubner et al., 2010). During mitosis, after nuclear envelope breakdown (NEBD), APC/C accumulates on mitotic spindles, centromeres, and centrosomes (Kraft et al., 2003; Acquaviva et al., 2004), reflecting a partially common localization with KIAA1430. Consistently, we confirmed the APC/C–KIAA1430 interaction in mitotically arrested, but not in interphase cells (Figure 4I). To functionally investigate the mitotic interaction, we used time-lapse microscopy to determine the time cells require from NEBD to the onset of anaphase as a function of APC/C activity. KIAA1430 knockdown resulted in a mild delay that was sensitive to reversine, a small molecule inhibitor of the mitotic checkpoint kinase MPS1 (Figures 4J and 4K) (Santaguida et al., 2010). These findings suggest that the depletion of KIAA1430 activates the spindle assembly checkpoint, thereby postponing the activation of the APC/C. Recent reports identified the ciliary protein hemingway as the *Drosophila* ortholog of KIAA1430 (Soulavie et al., 2014) and implicated the APC/C in regulating ciliary length and polarity (Ganner et al., 2009; Wang et al., 2014). Given that centrioles are common features of cilia and centrosomes, our data suggest that in human cells, KIAA1430 recruits a sub-fraction of the APC/C to the centrosome to facilitate mitotic progression.

These examples illustrate how the combination of three quantitative dimensions offers a unique view on the interactions of individual proteins that extends beyond their identification and facilitates their functional investigation.

We have compiled this information into an easily usable resource, provided as Data S1 and available via the IntAct database. For each of the 1,330 tagged cell lines, we present a concise, one-page summary outlining the abundance of the bait protein, the co-enrichment and confidence classification of candidate interactors along with the stoichiometry plot and the predictions of the core complexes. A reading guide is presented in Figure S5.

The Relevance of Substoichiometric Interactions

Our study revealed that interactions within obligate complexes constitute only a small minority of the interactome. We reasoned that the majority of remaining interactions should be of a functionally and conceptually different nature, as indicated by our example of the KIAA1430-APC/C interaction.

To investigate the interplay of the different types of interactions, we interrogated the chaperonin TRiC (also called CCT), which is known to act on a large number of client proteins (Hartl et al., 2011). Its core machinery of eight subunits was clearly identified as an abundant obligate complex (Figure 5A) and represents a prominent hub in our interactome dataset. Virtually all interactors co-enriched with tagged TRiC core subunits were co-chaperones, regulatory proteins of the phosducin family or proteins containing known substrate motifs (Yam et al., 2008) (Table

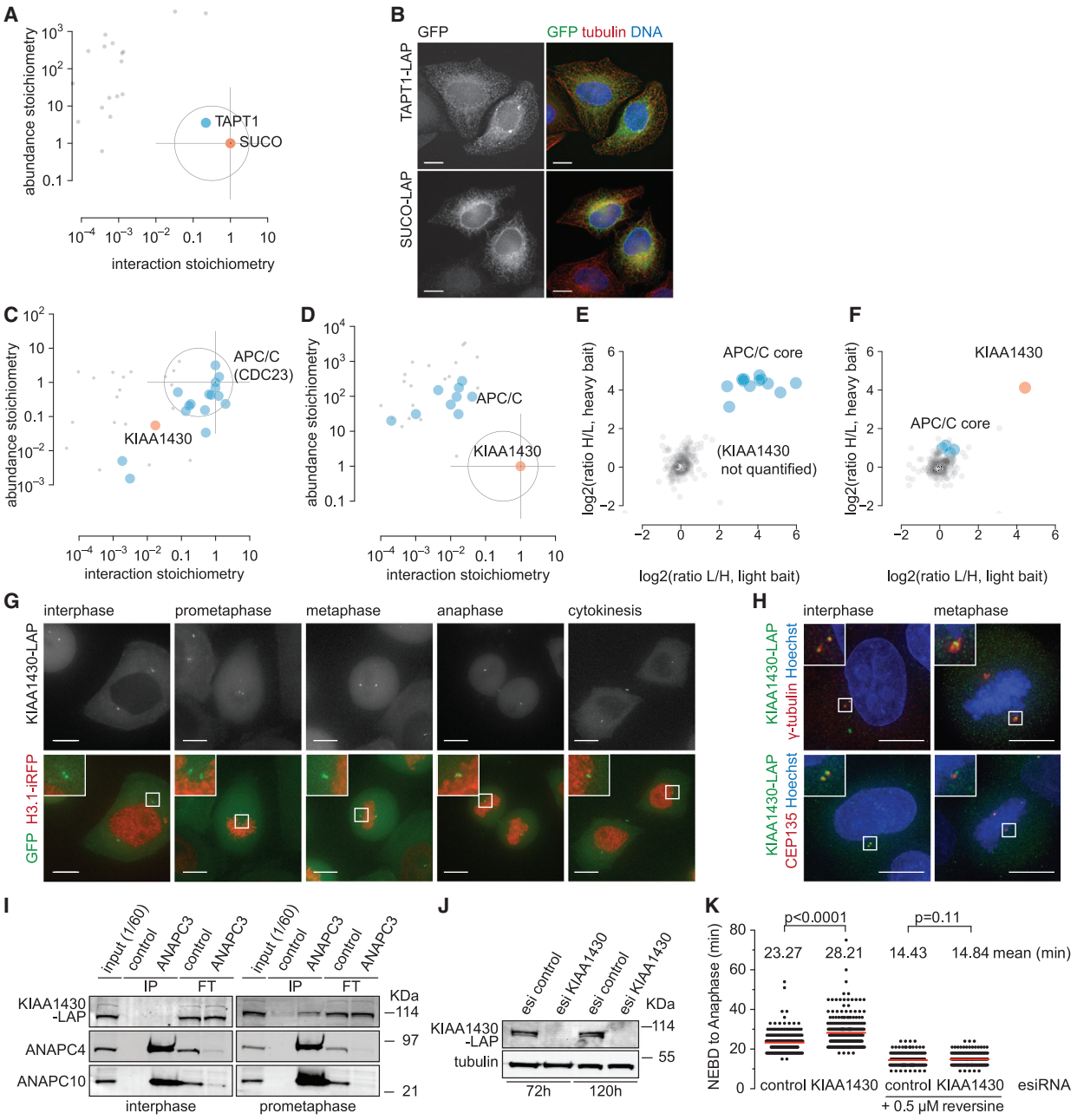

Figure 4. The TAPT1-SUCO Complex and the KIAA1430-APC/C Interaction

(A) Stoichiometry plot indicates stable TAPT1-SUCO complex.

(B) Immunofluorescence of TAPT1 and SUCO in HeLa shows ER localizations.

(C) Stoichiometry plot of APC/C interactors (bait: CDC23). Known core complex members (blue) and KIAA1430 (red) as novel substoichiometric interactor.

(D) Stoichiometry plot of KIAA1430 (red) interactors shows APC/C subunits (blue) as substoichiometric interactors.

(E) PAM-SILAC ratios plotted as medians of forward triplicate against label-swapped reverse triplicate (bait: CDC23).

(F) PAM-SILAC data using KIAA1430 as bait. Baits and stable interactors are recovered at ratios corresponding to label incorporation levels. Ratios of transient interactors are shifted toward 1:1.

(G) Maximum intensity projections of living interphase and mitotic cells expressing KIAA1430-LAP and histone 3.1-iRFP indicate that KIAA1430 localizes to centrioles.

(H) Co-localization of KIAA1430 with centrosomal marker γ-tubulin and the centriolar protein CEP135.

(I) Western blot analysis of ANAPC3 IPs and corresponding flow-throughs (FT) from interphase and mitotically arrested cells expressing KIAA1430-LAP.

(legend continued on next page)

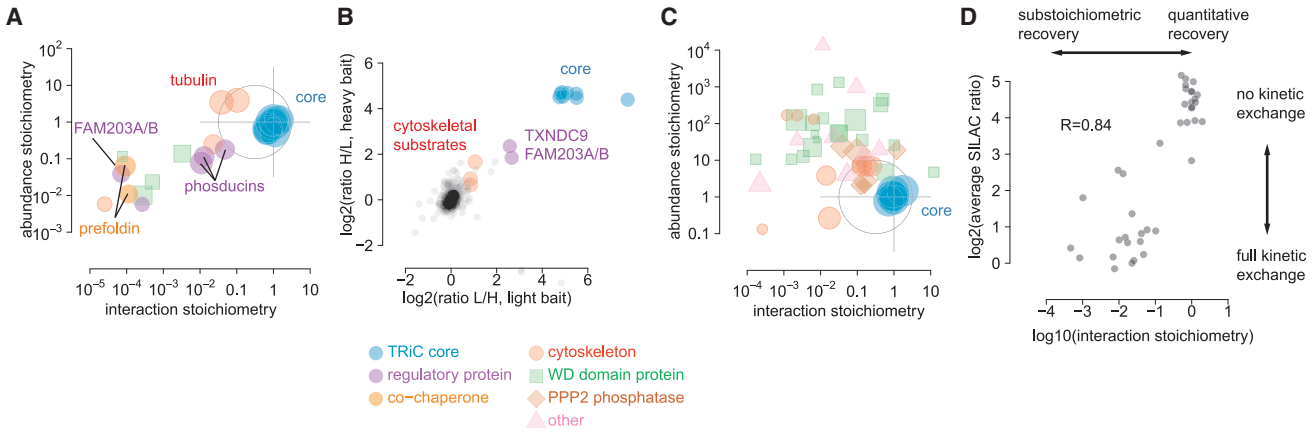

Figure 5. The TRiC Interactome Is Defined by Substoichiometric Links

(A) Stoichiometry plot of CCT3 interactors, representative of TRiC core subunits.

(B) PAM-SILAC results from the same bait protein.

(C) Reciprocal stoichiometry plot of averaged positions of the TRiC subunits from all bait pull-downs enriching at least three TRiC subunits. Symbol size indicates profile correlation. See also Tables S4 and S5.

(D) Systematic comparison of interaction stoichiometries and PAM-SILAC ratios for all interactions observed using CDC23, KIAA1430, and CCT3 as baits.

S4). Characteristic of all was a lower cellular abundance than TRiC (except for some cytoskeletal proteins) and substoichiometric recovery, classifying these interactors as distinct from the core subunits. When we performed a PAM-SILAC experiment to test for stable versus transient binding, the core complex composition that we had already established by the stoichiometry plot was confirmed, as these were all found to be stable binders (Figure 5B). Other interactors were transient, as their SILAC ratios indicated full dynamic exchange. Notable exceptions were some regulatory proteins and abundant cytoskeletal substrates, whose ratios lay between stable and fully dynamic binders. We consistently found the uncharacterized protein FAM203A/B as a substoichiometric interactor with intermediate dynamic exchange behavior. Its ortholog in *Caenorhabditis elegans* shows a cytoskeletal knockdown phenotype (Fievet et al., 2013). All of this was reminiscent of phosducin proteins, which TRiC requires to fold actin and tubulin (Hayes et al., 2011) and we therefore speculate that FAM203A/B might have a similar function.

In reciprocal interaction experiments, TRiC core complex members were co-enriched by ~5% of all bait proteins (Figure 5C; Table S5). This is in line with estimates of TRiC being involved in folding of 5%–10% of the proteome (Hartl et al., 2011). However, only some of these baits were also found in the reciprocal TRiC IPs. This asymmetry can be explained with knowledge of the underlying proteome: At 1.3 million copies of the hexadecameric complex, TRiC is much more abundant than most substrates, of which only a fraction will be in the process of folding at any given time (Table S3). Consequently, only a minute fraction of the TRiC pool will be acting on each substrate and its recovery will be "diluted" to substoichiometric levels. In the reciprocal case, however, TRiC occupies a significant fraction of the client protein population—the fraction in the state of folding—rendering the interaction more readily detectable within the dynamic range (Figure 5C).

The stoichiometry of TRiC recovery in the substrate IPs ranges from less than 10^{-3} to above 10^{-1} (Figure 5B). With TRiC substrates comprising 5%–10% of all protein molecules (a HeLa cell contains an estimated at 6×10^9 protein molecules), our stoichiometry data imply that on average 0.2%–0.4% of them are bound to the chaperone at any time. While substoichiometry may be thought to be of lower biological relevance, these interactions fulfil important functions as they connect very diverse set of protein classes. Moreover, our data also illustrate how the proteome-interactome relationship balances the amount of TRiC with the cumulative amount of its substrates.

Extrapolating from our APC/C, KIAA1430, and TRiC case studies, we investigated whether the different stoichiometric classifications of interactions carry over to other characteristics: first, we systematically compared interaction stoichiometries with dynamic exchange data for all interactions for which both orthogonal pieces of information were available (Figure 5D). There was almost perfect congruence of stoichiometric interactors with kinetically stably bound proteins and a surprisingly good overall correlation of substoichiometric recovery and the extent of dynamic exchange. This indicates that interaction stoichiometries are globally predictive of the biophysical stability of an interaction. Next, we investigated whether interaction stoichiometry is indicative of co-expression across tissues or cell types. We extracted protein abundance correlation profiles across

(J) Western analyses showing the extent of KIAA1430 depletion before and after the time-lapse analyses presented in (K).

(K) Time KIAA1430-depleted cells require to proceed from NEBD to anaphase, compared to control cells (n = 300 each); 0.5 μM reversine rescues the delay (n = 200 each). Red lines, mean. Significance according to two-tailed Mann-Whitney test. Scale bars, 10 μM.

See also Figure S4.

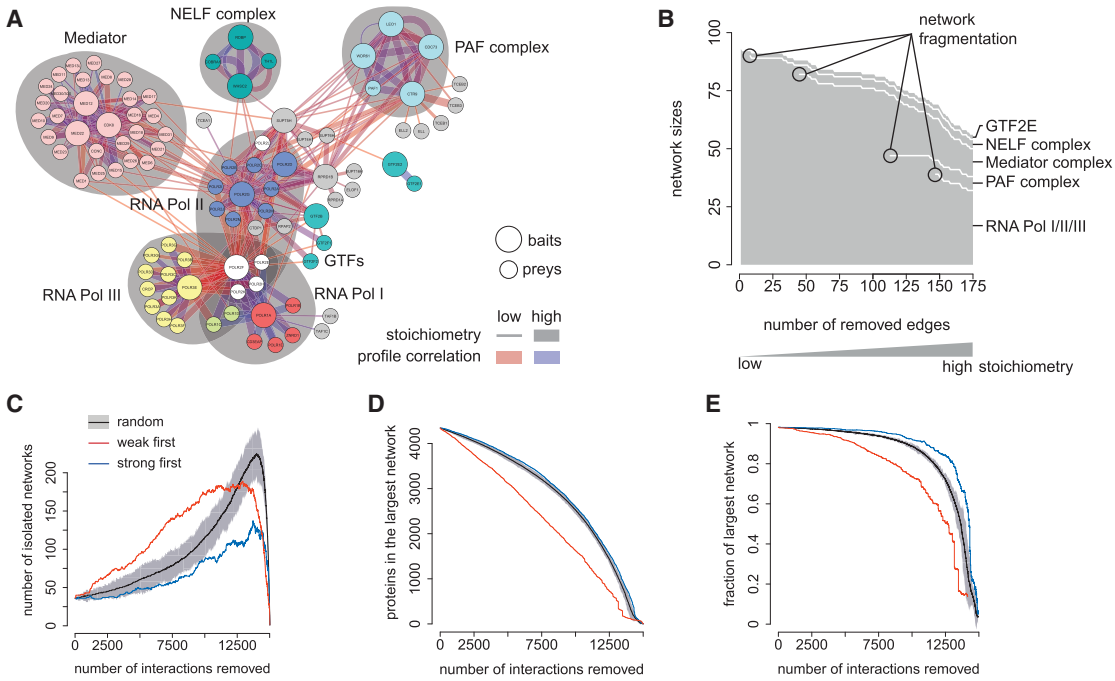

Figure 6. Strong and Weak Interactions Have Different Global Properties

(A) Sub-network of complexes surrounding RNA polymerases I/II/III. Proteins are colored by complex, edges by profile correlation, edge widths represent interaction stoichiometries.

(B) Effect of sequential removal of substoichiometric interactions on network sizes. Indicated are points where edge removal results in two fragmented sub-networks.

(C) Global network effect of random or targeted removal of interactions on the total number of isolated sub-networks.

(D) Effect on the number of proteins present in the largest entirely connected sub-network.

(E) Effect on the fraction of total connected proteins that are part of this largest sub-network.

See also Figure S6.

many tissues from a recent human proteome draft dataset (Kim et al., 2014). While co-expression coefficients scattered widely, there was still a notable relationship with interaction stoichiometry, with high-stoichiometry interactors more likely to be coherently expressed (Figure S6A). This is in agreement with earlier findings in yeast showing that members of stable complexes are enriched in co-regulated modules (Simonis et al., 2006). Conversely, substoichiometric interactions involve proteins that are not necessarily tightly co-regulated.

Finally, we tested whether interaction stoichiometry is predictive of the role of an interaction in network topology. We analyzed a sub-network of interactors surrounding RNA polymerases I, II, and III, recapitulating shared subunits and interactions with other complexes, such as general transcription factor complexes, the negative elongation factor (NELF) complex, the mediator complex, and the polymerase-associated factor (PAF) complex (Figure 6A). Sequential in silico removal of the most substoichiometric interactions from the network leads to fragmentation events, in which the individual complexes gradually lose their interconnections and emerge as individual modules (Figure 6B). Finally, the three polymerases remain internally connected via their shared subunits. Removing interactions in the reverse order does not lead to any network fragmentation, but rather results in roughly linear shrinkage of the network (Figure S6A).

Taking this approach to a global level, we probed the response of our entire network to the removal of edges according to their stoichiometry characteristics. Seminal studies on the topology of networks have shown that scale-free networks are resilient to random removal of edges, but sensitive to targeted attacks (Albert et al., 2000). Specifically, analysis of the network structure identifies the topologically most critical edges, removal of which leads to rapid network fragmentation.

In our case, we targeted edges for removal solely by their "local" interaction stoichiometry readout, agnostic to their global network roles. We removed edges sequentially, starting at either the lowest or highest interaction stoichiometry, comparing this with random removal of edges.

This revealed vastly different network responses (Figure 6C). The most substoichiometric interactions turned out to be most critical for network topology: Their preferential removal led to a rapid increase of the number of isolated network fragments, whereas removing the strongest 50% of edges hardly resulted in any network fragmentation (Figure 6C). The largest connected component, which causes the typical "hairball" appearance of large-scale networks, shrunk about linearly with removal of weak interactions (Figure 6D) and also left more proteins entirely unconnected (Figure S6A). Conversely, preferential removal of edges from the other end of the stoichiometry scale led to a

network response that increased its small-world characteristics: the largest network encompasses the vast majority of connected proteins (Figure 6E), fewer proteins are left without connections (Figure S6B) and isolated network fragments are smaller (Figure S6C). Similar patterns of network response were observed in a study analyzing mobile phone communication networks by removing the strongest versus the weakest interactions (Onnela et al., 2007). In analogy to that study, and based on our findings of the relationship between interaction stoichiometries and kinetic stabilities (Figure 5D), we propose a strong/weak terminology for interaction stoichiometries and term interactions with near-stoichiometric recovery of the prey "strong" and substoichiometric interactors "weak."

Together, our analyses show that interaction stoichiometries, which are local properties derived from single interaction experiments, predict the global behavior of the proteins involved: strong interactions are indicative of proteins that are co-regulated across cell types. In the network, they form modules of high interconnectivity, rendering the network topologically resilient to their removal. Weak interactions, on the other hand, dominate the network both in numbers and by their topologically critical role as long-range interactions between more diverse sets of proteins. As a consequence, interaction networks can be fragmented into individual, defined modules, by identifying and removing weak links. In summary, availability of interaction stoichiometries on a global scale effectively allows us to "comb" the interactome hairball, to identify modules, and visualize their interconnectedness.

DISCUSSION

Here, we have introduced a novel concept of interactome analysis. Using an efficient, low-stringent IP protocol, accurate label-free quantification of both the IPs and the complete proteome, we extracted three quantitative dimensions, all of which proved critical for characterizing protein interactions. While the first dimension identifies statistically significant interactions, the second and third dimension define their stoichiometric contexts. Earlier large-scale studies did not include or interpret these additional dimensions, in part because of the challenges involved in extracting accurate quantitative values. Moreover, past studies often employed overexpression of bait proteins, precluding meaningful stoichiometry readout (Gibson et al., 2013), and near-complete proteome coverage was also often not attainable.

Finding stable protein complexes is usually a major goal of interactomics studies. We showed that obligate protein complexes feature a unique signature of balanced stoichiometries—an infrequent occurrence among the multitude of interactions. Such a signature led us to discover the TAPT1-SUCO complex in the ER membrane. This complex ties together a body of available evidence, including knockout phenotypes of both TAPT1 and SUCO and genetic interactions of their yeast orthologs. As a representative of the majority of weaker, non-obligate interactions, we characterized the binding of KIAA1430 to the APC/C, suggesting that low interaction stoichiometries are the result of an interaction that is limited to centrioles in mitotic cells and biophysically weaker than interactions between APC/C core members. Furthermore, our stoichiometry-based classification subdivided the interactome of the TRiC chaperonin into obligate core complex subunits, regulatory interactors, and a large number of substrates. We found that lack of reciprocal verification can be indicative of an inherently asymmetric nature of biologically relevant interactions, particularly outside obligate core complexes. This example also illustrates how the observed interactome is shaped by protein abundances and, conversely, implies overall regulation of protein abundances by protein interactions. Therefore, the interactome always has to be interpreted as a function of the underlying proteome.

We have shown that interaction stoichiometries generally correlate with the biophysical stability of an interaction. Weak interactions have frequently gone undetected in interactome studies and may be thought to be less important; nevertheless they are crucial features of networks in general and social networks in particular (Granovetter, 1973; Csermely, 2006). Our study directly and quantitatively demonstrates the predominance of weak interactions in the protein interactome. MS-based methods cover more than four orders of magnitude of interaction stoichiometry (Collins et al., 2013), and our low-stringency biochemical workflow ideally harnesses this sensitivity. However, substoichiometric interactions involving low abundance preys can still be challenging to detect (Figures S3D and S3E). Therefore, the prevalence of weak interactions is likely to be even more pronounced and their relevance vastly underappreciated.

Previous studies typically counted all interactions as equal, once they had been accepted based on their statistical parameters or scores. Therefore, the roles of individual interactions had to be predicted from prior knowledge or from global network properties. Highly connected proteins were described as interaction hubs, regions of high clustering coefficients with many shared pathway annotations were characterized as complexes (Collins et al., 2007; Hart et al., 2007), and weak interactions were inferred from weaker connectivity patterns (Malovannaya et al., 2011). However, limited coverage of the interactome is a confounding factor for such strategies.

In contrast, we here have shown directly that local stoichiometry data reflect global network topological properties of interactions, setting the stage for quantitative network analysis from the ground up.

Substoichiometric interactions form the "glue" that holds the cellular network together—as shown specifically for the RNA polymerase network and globally for the entire network—and are hence critical for network structure. This property, which may seem counterintuitive at first, prompted us to propose interaction stoichiometry as a measure of interaction strength. Of note, a range of underlying mechanisms can cause a weak interaction according to this terminology, for instance low biophysical affinity, high kinetic exchange rates, limited spatiotemporal overlap of interactors, or indirect interactions that are bridged via other biomolecules, all of which may result in a substoichiometric readout. If such weak links are removed from the network, it collapses into defined modules that are tightly interconnected by the remaining strong links. Translated into biological terms, stable complexes would remain in isolation, but without weak links, they would not be able to connect to each other or to transient, dynamic regulators.

A major contribution of this study lies in the characterization of the interactomes surrounding more than 1,100 different baits, which together cover a large part of the expressed proteome with more than 28,000 interactions. We present our results in an accessible format that can be easily mined and interpreted by non-specialists. Our resource of mammalian cell lines expressing GFP-tagged proteins under endogenous control can be employed for other studies (e.g., focusing on subcellular localization or functional characterization of individual proteins). The interaction data validate these cell lines for such uses and the use of mouse orthologs as surrogates. They also imply remarkably similar protein interactomes between human and mouse.

We approach saturation with respect to the number of proteins that can be covered (Figure S6D), but observe only part of the entire interactome directly, which our data predicts to encompass between 80,000 and 180,000 detectable interactions in HeLa (Figure S6E). Our additional quantitative dimensions may prove helpful for increasing interactome coverage in silico, for example, by selective matrix expansion (Seebacher and Gavin, 2011). Given its usefulness in interpreting interaction data, the stoichiometry readout developed here can become a general basis for future interactome studies and for the analysis of interactome dynamics, which will manifest foremost as quantitative alteration of occupancies rather than qualitative gain or loss of interactors.

EXPERIMENTAL PROCEDURES

Cell Culture

HeLa Kyoto cell lines expressing N- or C-terminally tagged proteins from BAC transgenes were generated, cultured, and imaged as previously described (Poser et al., 2008). Tags are based on the "localization and affinity purification" (LAP) tag, consisting of GFP and a functionalized linker. All BAC cell lines and tag sequences are listed in Table S1 along with proteome and interactome metadata on the bait proteins. Cells were grown to near-confluency on two 15-cm cell culture dishes per interaction experiment, detached with Accutase, and snap frozen. Three replicates were harvested in at least two different passages.

Affinity Purification and Mass Spectrometry

Cell pellets were lysed and subjected to affinity purification on a robotic system, followed by single-shot mass spectrometric analysis on an Orbitrap instrument (Hubner et al., 2010). We processed triplicates separately on different days and carried out MS-analyses in randomized order over the course of weeks to months.

Whole Proteome Measurements

HeLa cells were lysed in guanidinium chloride lysis buffer and digested sequentially with LysC and trypsin as described (Kulak et al., 2014). Peptides were desalted on stacked C18 reverse phase (Waters Sep-Pak) and strong cation exchange cartridges and eluted using 70% acetonitrile. Pooled eluates were separated into six fractions on strong anion exchange (SAX) StageTips (Wiśniewski et al., 2010). MS measurements were performed in three replicates on a quadrupole Orbitrap mass spectrometer (Kulak et al., 2014).

Data Processing

Raw files were processed with MaxQuant (Cox and Mann, 2008) (version 1.3.9.10) in several sets, each containing ~600 randomly assigned AP-MS runs and the HeLa proteome fractions. Tandem mass spectrometry (MS/MS) spectra were searched against a modified version of the November 2012 release of the UniProt complete human proteome sequence database. For each bait protein expressed from a mouse BAC locus, the human sequence in the fasta file was concatenated with the mouse sequence (unless identical). Human identifiers were used for mapping purposes. We used MaxLFQ, MaxQuant's label-free quantification (LFQ) algorithm to calculate protein intensity profiles across samples (Cox et al., 2014). We required one ratio count for each pairwise comparison step and activated the FastLFQ setting with two minimum and two average comparisons to enable the normalization of large datasets in manageable computing time.

Detection of Protein Interactions

Protein identifications were filtered, removing hits to the reverse decoy database as well as proteins only identified by modified peptides. We required that each protein be quantified in all replicates from the AP-MS samples of at least one cell line. Protein LFQ intensities were logarithmized and missing values imputed by values simulating noise around the detection limit. For each protein, a non-parametric method was used to select a subset of samples that provide a distribution of background intensities for this protein (Supplemental Experimental Procedures). This subset was used first to normalize all protein intensities to represent relative enrichment and then to serve as the control group for a two-tailed Welch's t test. Specific outliers in the volcano plots of logarithmized p values against enrichments were determined by an approach making use of the asymmetry in the outlier population (Figures S1E and S1F). We used two cut-offs of different stringencies, representing 1% and 5% of enrichment false discovery rate (FDR), respectively. Correlation coefficients between the intensity profiles of interacting proteins were calculated as additional quality parameters (Keilhauer et al., 2015). Enrichment FDR (classes A–C) and profile correlation (modifier + or –) define the confidence class of an interaction (Figure S1G).

Interaction Stoichiometries and Cellular Copy Numbers

Estimating interaction stoichiometries requires the comparison of the amounts of different proteins relative to each other in one IP. We first subtracted the median intensity across all samples to account for background binding. We then divided LFQ intensities by the number of theoretically observable peptides for this protein (Schwanhäusser et al., 2011). Finally, we expressed stoichiometries relative to the bait protein. Cellular copy numbers and abundances were calculated using a similar approach (Wiśniewski et al., 2014) on the whole proteome data and brought to absolute scale by normalization to a total protein amount of 200 pg in a cell volume of 1 pl for a HeLa cell.

Network Analyses

Network analyses were performed based on the data listed in Table S2. For the purpose of counting unique interactions and for the histogram of the numbers of interactors, we regarded interactions as non-directional, flattened multiple protein groups mapping to the same gene name and to the most abundant isoform and considered interactions found multiple times only once. For network perturbation analyses, we selected all non-self-interactions of confidence classes A+, A, and B+ and assembled them into graphs. We then removed edges sequentially according to their interaction stoichiometry readout. Prey-bait combinations discovered multiple times were treated as separate edges. Once a protein had lost all its edges, it was removed. As control, we deleted edges randomly and represented the median of 100 random repetitions and represent the scatter as the first or third quartile ±1.5 interquartile ranges.

ACCESSION NUMBERS

The accession number for the protein interaction data reported in this paper, submitted through IntAct (Orchard et al., 2014), to the IMEx Consortium (http://www.imexconsortium.org): IM-24272. The accession numbers for the raw mass spectrometric data, deposited via PRIDE (Vizcaino et al., 2013) to the ProteomeXchange Consortium (http://proteomecentral.proteomexchange.org): PXD002815 and PXD002829.

SUPPLEMENTAL INFORMATION

Supplemental Information includes Supplemental Experimental Procedures, six figures, five tables, and one data set and can be found with this article online at http://dx.doi.org/10.1016/j.cell.2015.09.053.

AUTHOR CONTRIBUTIONS

M.Y.H. did the experiments, conceived and implemented the bioinformatics methods, and analyzed and interpreted the data. N.C.H. developed the QUBIC pipeline in a high throughput format. J.C. developed the MaxQuant software modules for label-free quantification of very large datasets and contributed to data analysis. N.N. provided the whole proteome data. I.P. and Y.T. generated the BAC-GFP cell lines. I.P. performed fluorescence microscopy and western blot analyses. I.A.G., I.W., and J.M. generated the data shown in Figures 4G–4K. J.M. and F.B. conceived, supervised, and interpreted the experiments in Figures 4G–4K. M.M. and A.A.H. conceived the study and supervised the experiments. M.Y.H. and M.M. wrote the manuscript.

ACKNOWLEDGMENTS

This work was performed within the project framework of the German medical genome research funded by the Federal Ministry of Education and Research (FKZ01GS0861, DiGtoP). We acknowledge funding from the Max Planck Society and the European Commission's Sixth and Seventh Framework Programs (FP6-LSHG-CT-2004-503464, MitoCheck; FP7-HEALTH-F4-2008-201648, PROSPECTS; FP7-HEALTH-2009-241548, MitoSys). J.M. is supported by the German Research Foundation (DFG) (Emmy Noether, MA 5831/1-1), I.A.G. is a member of the DIGS-BB PhD program. Antibodies for BAC validation were a gift from C. Stadler and E. Lundberg. We thank M. Leuschner, A. Ssykor, M. Augsburg, A. Schwager, M.T. Pham, G. Sowa, K. Mayr, I. Paron, B. Splettstößer, D. Vogg, B. Chatterjee, M. Grötzinger, and S. Kroiß for technical assistance. C. Schaab, S. Schloissnig, P. Porras, and M. Oroshi provided bioinformatics support. We thank M. Sarov, M. Seiler, M.C. Bassik, S. Pinkert, A. Bracher, H.C. Eberl, T. Viturawong, E.C. Keilhauer, A. Hrle, G. Pichler, N.A. Kulak, and M. Räschle for helpful discussions.

Received: February 5, 2015
Revised: July 6, 2015
Accepted: September 17, 2015
Published: October 22, 2015

REFERENCES

Acquaviva, C., Herzog, F., Kraft, C., and Pines, J. (2004). The anaphase promoting complex/cyclosome is recruited to centromeres by the spindle assembly checkpoint. Nat. Cell Biol. *6*, 892–898.

Albert, R., Jeong, H., and Barabasi, A.L. (2000). Error and attack tolerance of complex networks. Nature *406*, 378–382.

Bantscheff, M., Lemeer, S., Savitski, M.M., and Kuster, B. (2012). Quantitative mass spectrometry in proteomics: critical review update from 2007 to the present. Anal. Bioanal. Chem. *404*, 939–965.

Bassik, M.C., Kampmann, M., Lebbink, R.J., Wang, S., Hein, M.Y., Poser, I., Weibezahn, J., Horlbeck, M.A., Chen, S., Mann, M., et al. (2013). A systematic mammalian genetic interaction map reveals pathways underlying ricin susceptibility. Cell *152*, 909–922.

Beck, M., Claassen, M., and Aebersold, R. (2011). Comprehensive proteomics. Curr. Opin. Biotechnol. *22*, 3–8.

Collins, S.R., Kemmeren, P., Zhao, X.C., Greenblatt, J.F., Spencer, F., Holstege, F.C., Weissman, J.S., and Krogan, N.J. (2007). Toward a comprehensive atlas of the physical interactome of Saccharomyces cerevisiae. Mol. Cell. Proteomics *6*, 439–450.

Collins, B.C., Gillet, L.C., Rosenberger, G., Röst, H.L., Vichalkovski, A., Gstaiger, M., and Aebersold, R. (2013). Quantifying protein interaction dynamics by SWATH mass spectrometry: application to the 14-3-3 system. Nat. Methods *10*, 1246–1253.

Cox, J., and Mann, M. (2008). MaxQuant enables high peptide identification rates, individualized p.p.b.-range mass accuracies and proteome-wide protein quantification. Nat. Biotechnol. *26*, 1367–1372.

Cox, J., Hein, M.Y., Luber, C.A., Paron, I., Nagaraj, N., and Mann, M. (2014). Accurate proteome-wide label-free quantification by delayed normalization and maximal peptide ratio extraction, termed MaxLFQ. Mol. Cell. Proteomics *13*, 2513–2526.

Csermely, P. (2006). Weak Links: Stabilizers of Complex Systems from Proteins to Social Networks, First Edition (Springer).

Ewing, R.M., Chu, P., Elisma, F., Li, H., Taylor, P., Climie, S., McBroom-Cerajewski, L., Robinson, M.D., O'Connor, L., Li, M., et al. (2007). Large-scale mapping of human protein-protein interactions by mass spectrometry. Mol. Syst. Biol. *3*, 89.

Fievet, B.T., Rodriguez, J., Naganathan, S., Lee, C., Zeiser, E., Ishidate, T., Shirayama, M., Grill, S., and Ahringer, J. (2013). Systematic genetic interaction screens uncover cell polarity regulators and functional redundancy. Nat. Cell Biol. *15*, 103–112.

Friederichs, J.M., Gardner, J.M., Smoyer, C.J., Whetstine, C.R., Gogol, M., Slaughter, B.D., and Jaspersen, S.L. (2012). Genetic analysis of Mps3 SUN domain mutants in Saccharomyces cerevisiae reveals an interaction with the SUN-like protein Slp1. G3 (Bethesda) *2*, 1703–1718.

Ganner, A., Lienkamp, S., Schäfer, T., Romaker, D., Wegierski, T., Park, T.J., Spreitzer, S., Simons, M., Gloy, J., Kim, E., et al. (2009). Regulation of ciliary polarity by the APC/C. Proc. Natl. Acad. Sci. USA *106*, 17799–17804.

Gibson, T.J., Seiler, M., and Veitia, R.A. (2013). The transience of transient overexpression. Nat. Methods *10*, 715–721.

Gingras, A.C., Gstaiger, M., Raught, B., and Aebersold, R. (2007). Analysis of protein complexes using mass spectrometry. Nat. Rev. Mol. Cell Biol. *8*, 645–654.

Granovetter, M.S. (1973). The Strength of Weak Ties. Am. J. Sociol. *78*, 1360–1380.

Hart, G.T., Lee, I., and Marcotte, E.R. (2007). A high-accuracy consensus map of yeast protein complexes reveals modular nature of gene essentiality. BMC Bioinformatics *8*, 236.

Hartl, F.U., Bracher, A., and Hayer-Hartl, M. (2011). Molecular chaperones in protein folding and proteostasis. Nature *475*, 324–332.

Hauri, S., Wepf, A., van Drogen, A., Varjosalo, M., Tapon, N., Aebersold, R., and Gstaiger, M. (2013). Interaction proteome of human Hippo signaling: modular control of the co-activator YAP1. Mol. Syst. Biol. *9*, 713.

Havugimana, P.C., Hart, G.T., Nepusz, T., Yang, H., Turinsky, A.L., Li, Z., Wang, P.I., Boutz, D.R., Fong, V., Phanse, S., et al. (2012). A census of human soluble protein complexes. Cell *150*, 1068–1081.

Hayes, N.V.L., Jossé, L., Smales, C.M., and Carden, M.J. (2011). Modulation of phosducin-like protein 3 (PhLP3) levels promotes cytoskeletal remodelling in a MAPK and RhoA-dependent manner. PLoS ONE *6*, e28271.

Hein, M.Y., Sharma, K., Cox, J., and Mann, M. (2013). Proteomic Analysis of Cellular Systems. In Handbook of Systems Biology, *Chapter 1*, Walhout A.J.M., Vidal M., and Dekker J., eds. (Academic Press), pp. 3–25.

Howell, G.R., Shindo, M., Murray, S., Gridley, T., Wilson, L.A., and Schimenti, J.C. (2007). Mutation of a ubiquitously expressed mouse transmembrane protein (Tapt1) causes specific skeletal homeotic transformations. Genetics *175*, 699–707.

Hubner, N.C., Bird, A.W., Cox, J., Splettstoesser, B., Bandilla, P., Poser, I., Hyman, A., and Mann, M. (2010). Quantitative proteomics combined with BAC TransgeneOmics reveals in vivo protein interactions. J. Cell Biol. *189*, 739–754.

Huh, W.K., Falvo, J.V., Gerke, L.C., Carroll, A.S., Howson, R.W., Weissman, J.S., and O'Shea, E.K. (2003). Global analysis of protein localization in budding yeast. Nature *425*, 686–691.

Hutchins, J.R., Toyoda, Y., Hegemann, B., Poser, I., Hériché, J.K., Sykora, M.M., Augsburg, M., Hudecz, O., Buschhorn, B.A., Bulkescher, J., et al. (2010). Systematic analysis of human protein complexes identifies chromosome segregation proteins. Science *328*, 593–599.

Jonikas, M.C., Collins, S.R., Denic, V., Oh, E., Quan, E.M., Schmid, V., Weibezahn, J., Schwappach, B., Walter, P., Weissman, J.S., and Schuldiner, M. (2009). Comprehensive characterization of genes required for protein folding in the endoplasmic reticulum. Science *323*, 1693–1697.

Kachroo, A.H., Laurent, J.M., Yellman, C.M., Meyer, A.G., Wilke, C.O., and Marcotte, E.M. (2015). Evolution. Systematic humanization of yeast genes reveals conserved functions and genetic modularity. Science *348*, 921–925.

Keilhauer, E.C., Hein, M.Y., and Mann, M. (2015). Accurate protein complex retrieval by affinity enrichment mass spectrometry (AE-MS) rather than affinity purification mass spectrometry (AP-MS). Mol. Cell. Proteomics *14*, 120–135.

Kim, M.S., Pinto, S.M., Getnet, D., Nirujogi, R.S., Manda, S.S., Chaerkady, R., Madugundu, A.K., Kelkar, D.S., Isserlin, R., Jain, S., et al. (2014). A draft map of the human proteome. Nature *509*, 575–581.

Kittler, R., Pelletier, L., Ma, C., Poser, I., Fischer, S., Hyman, A.A., and Buchholz, F. (2005). RNA interference rescue by bacterial artificial chromosome transgenesis in mammalian tissue culture cells. Proc. Natl. Acad. Sci. USA *102*, 2396–2401.

Kraft, C., Herzog, F., Gieffers, C., Mechtler, K., Hagting, A., Pines, J., and Peters, J.M. (2003). Mitotic regulation of the human anaphase-promoting complex by phosphorylation. EMBO J. *22*, 6598–6609.

Kristensen, A.R., Gsponer, J., and Foster, L.J. (2012). A high-throughput approach for measuring temporal changes in the interactome. Nat. Methods *9*, 907–909.

Kulak, N.A., Pichler, G., Paron, I., Nagaraj, N., and Mann, M. (2014). Minimal, encapsulated proteomic-sample processing applied to copy-number estimation in eukaryotic cells. Nat. Methods *11*, 319–324.

Maliga, Z., Junqueira, M., Toyoda, Y., Ettinger, A., Mora-Bermúdez, F., Klemm, R.W., Vasilj, A., Guhr, E., Ibarlucea-Benitez, I., Poser, I., et al. (2013). A genomic toolkit to investigate kinesin and myosin motor function in cells. Nat. Cell Biol. *15*, 325–334.

Malovannaya, A., Lanz, R.B., Jung, S.Y., Bulynko, Y., Le, N.T., Chan, D.W., Ding, C., Shi, Y., Yucer, N., Krenciute, G., et al. (2011). Analysis of the human endogenous coregulator complexome. Cell *145*, 787–799.

Mann, M., Kulak, N.A., Nagaraj, N., and Cox, J. (2013). The coming age of complete, accurate, and ubiquitous proteomes. Mol. Cell *49*, 583–590.

Mellacheruvu, D., Wright, Z., Couzens, A.L., Lambert, J.P., St-Denis, N.A., Li, T., Miteva, Y.V., Hauri, S., Sardiu, M.E., Low, T.Y., et al. (2013). The CRAPome: a contaminant repository for affinity purification-mass spectrometry data. Nat. Methods *10*, 730–736.

Onnela, J.P., Saramäki, J., Hyvönen, J., Szabó, G., Lazer, D., Kaski, K., Kertész, J., and Barabási, A.L. (2007). Structure and tie strengths in mobile communication networks. Proc. Natl. Acad. Sci. USA *104*, 7332–7336.

Orchard, S., Ammari, M., Aranda, B., Breuza, L., Briganti, L., Broackes-Carter, F., Campbell, N.H., Chavali, G., Chen, C., del-Toro, N., et al. (2014). The MIntAct project—IntAct as a common curation platform for 11 molecular interaction databases. Nucleic Acids Res. *42*, D358–D363.

Phillips-Krawczak, C.A., Singla, A., Starokadomskyy, P., Deng, Z., Osborne, D.G., Li, H., Dick, C.J., Gomez, T.S., Koenecke, M., Zhang, J.S., et al. (2015). COMMD1 is linked to the WASH complex and regulates endosomal trafficking of the copper transporter ATP7A. Mol. Biol. Cell *26*, 91–103.

Poser, I., Sarov, M., Hutchins, J.R., Hériché, J.K., Toyoda, Y., Pozniakovsky, A., Weigl, D., Nitzsche, A., Hegemann, B., Bird, A.W., et al. (2008). BAC TransgeneOmics: a high-throughput method for exploration of protein function in mammals. Nat. Methods *5*, 409–415.

Rolland, T., Taşan, M., Charloteaux, B., Pevzner, S.J., Zhong, Q., Sahni, N., Yi, S., Lemmens, I., Fontanillo, C., Mosca, R., et al. (2014). A proteome-scale map of the human interactome network. Cell *159*, 1212–1226.

Rual, J.F., Venkatesan, K., Hao, T., Hirozane-Kishikawa, T., Dricot, A., Li, N., Berriz, G.F., Gibbons, F.D., Dreze, M., Ayivi-Guedehoussou, N., et al. (2005). Towards a proteome-scale map of the human protein-protein interaction network. Nature *437*, 1173–1178.

Ruepp, A., Waegele, B., Lechner, M., Brauner, B., Dunger-Kaltenbach, I., Fobo, G., Frishman, G., Montrone, C., and Mewes, H.W. (2010). CORUM: the comprehensive resource of mammalian protein complexes–2009. Nucleic Acids Res. *38*, D497–D501.

Santaguida, S., Tighe, A., D'Alise, A.M., Taylor, S.S., and Musacchio, A. (2010). Dissecting the role of MPS1 in chromosome biorientation and the spindle checkpoint through the small molecule inhibitor reversine. J. Cell Biol. *190*, 73–87.

Schwanhäusser, B., Busse, D., Li, N., Dittmar, G., Schuchhardt, J., Wolf, J., Chen, W., and Selbach, M. (2011). Global quantification of mammalian gene expression control. Nature *473*, 337–342.

Seebacher, J., and Gavin, A.C. (2011). SnapShot: Protein-protein interaction networks. Cell *144*, 1000.

Simonis, N., Gonze, D., Orsi, C., van Helden, J., and Wodak, S.J. (2006). Modularity of the transcriptional response of protein complexes in yeast. J. Mol. Biol. *363*, 589–610.

Smits, A.H., Jansen, P.W., Poser, I., Hyman, A.A., and Vermeulen, M. (2012). Stoichiometry of chromatin-associated protein complexes revealed by label-free quantitative mass spectrometry-based proteomics. Nucleic Acids Res. *41*, e28.

Sohaskey, M.L., Jiang, Y., Zhao, J.J., Mohr, A., Roemer, F., and Harland, R.M. (2010). Osteopotentia regulates osteoblast maturation, bone formation, and skeletal integrity in mice. J. Cell Biol. *189*, 511–525.

Soulavie, F., Piepenbrock, D., Thomas, J., Vieillard, J., Duteyrat, J.L., Cortier, E., Laurençon, A., Göpfert, M.C., and Durand, B. (2014). hemingway is required for sperm flagella assembly and ciliary motility in Drosophila. Mol. Biol. Cell *25*, 1276–1286.

Stelzl, U., Worm, U., Lalowski, M., Haenig, C., Brembeck, F.H., Goehler, H., Stroedicke, M., Zenkner, M., Schoenherr, A., Koeppen, S., et al. (2005). A human protein-protein interaction network: a resource for annotating the proteome. Cell *122*, 957–968.

Turner, B., Razick, S., Turinsky, A.L., Vlasblom, J., Crowdy, E.K., Cho, E., Morrison, K., Donaldson, I.M., and Wodak, S.J. (2010). iRefWeb: interactive analysis of consolidated protein interaction data and their supporting evidence. Database (Oxford) *2010*, baq023.

Vizcaino, J.A., Cote, R.G., Csordas, A., Dianes, J.A., Fabregat, A., Foster, J.M., Griss, J., Alpi, E., Birim, M., Contell, J., et al. (2013). The PRoteomics IDEntifications (PRIDE) database and associated tools: status in 2013. Nucleic Acids Res. *41*, D1063–D1069.

Wang, X., and Huang, L. (2008). Identifying dynamic interactors of protein complexes by quantitative mass spectrometry. Mol. Cell. Proteomics *7*, 46–57.

Wang, W., Wu, T., and Kirschner, M.W. (2014). The master cell cycle regulator APC-Cdc20 regulates ciliary length and disassembly of the primary cilium. eLife *3*, e03083.

Wepf, A., Glatter, T., Schmidt, A., Aebersold, R., and Gstaiger, M. (2009). Quantitative interaction proteomics using mass spectrometry. Nat. Methods *6*, 203–205.

Wiśniewski, J.R., Nagaraj, N., Zougman, A., Gnad, F., and Mann, M. (2010). Brain phosphoproteome obtained by a FASP-based method reveals plasma membrane protein topology. J. Proteome Res. *9*, 3280–3289.

Wiśniewski, J.R., Hein, M.Y., Cox, J., and Mann, M. (2014). A "proteomic ruler" for protein copy number and concentration estimation without spike-in standards. Mol. Cell. Proteomics *13*, 3497–3506.

Yam, A.Y., Xia, Y., Lin, H.T., Burlingame, A., Gerstein, M., and Frydman, J. (2008). Defining the TRiC/CCT interactome links chaperonin function to stabilization of newly made proteins with complex topologies. Nat. Struct. Mol. Biol. *15*, 1255–1262.

Cell

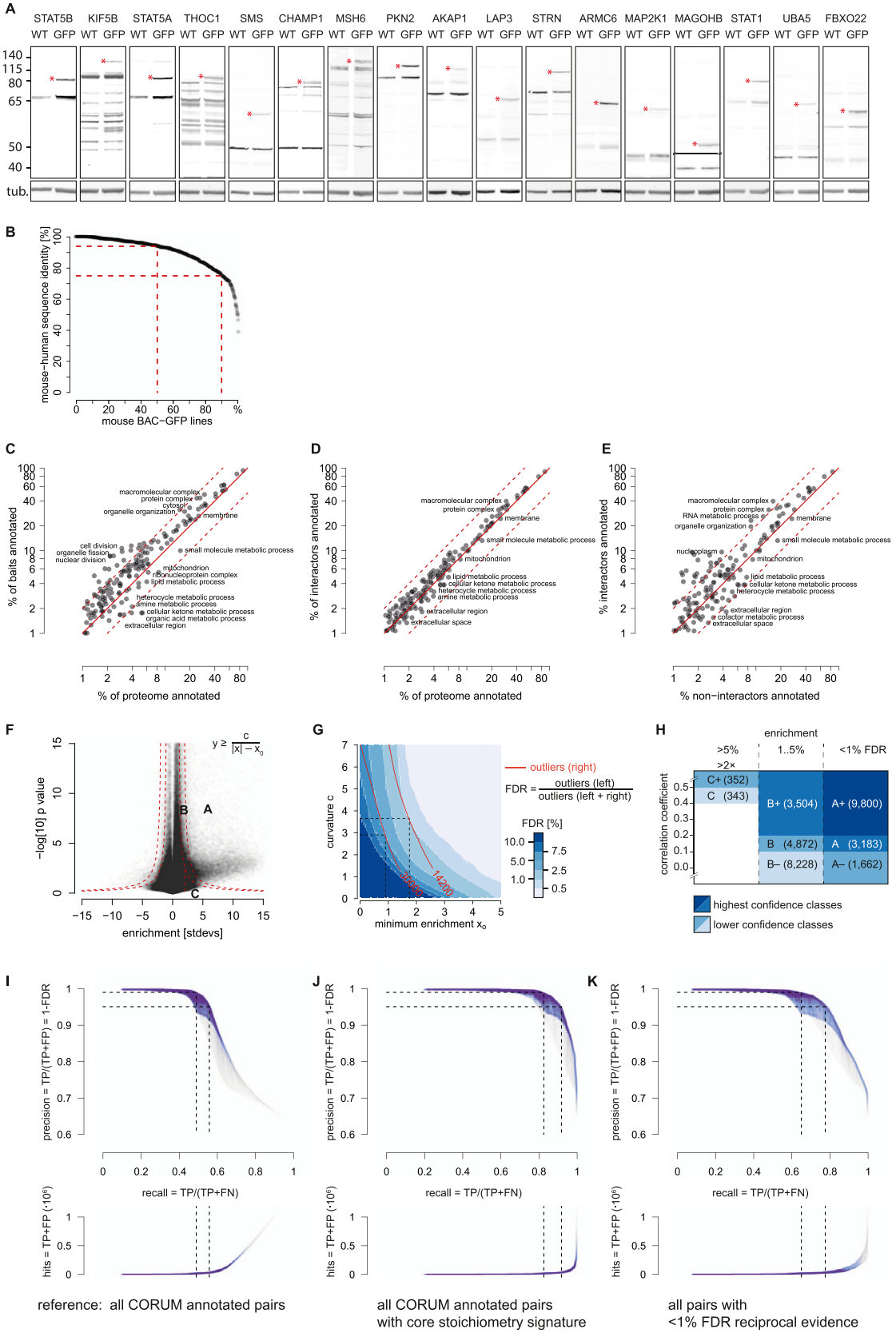

(legend on next page)

Figure S1. Properties of the Cell Line Resource and Statistical Methods, Related to Figure 1

(A) Representative western blot panel of parental HeLa line (left lanes) compared to BAC-GFP lines (right lanes), probed with antibodies against the individual bait proteins, and against tubulin as loading control. The GFP-tagged proteins, which are absent in the parental line (marked with asterisks), are expressed around or below the levels of their untagged endogenous counterparts, migrating at ~30kDa lower molecular mass.

(B) Amino acid sequence identities for BAC-GFP lines expressing tagged proteins from the mouse locus. Median sequence identity between mouse and human is 94%, and 90% of all mouse BAC lines show sequence identities greater 75%.

(C–E) Test for biases of the selection of baits as well as interacting and non-interacting proteins compared to the HeLa proteome by Gene Ontology (GO) Slim annotations. We calculated the percentages of all annotations that apply to > 1% of all proteins. The red solid line indicates no bias. Dashed lines indicate 2-fold over- or underrepresentation. (C) The selection of bait proteins shows a slight enrichment of annotated, well-studied proteins. Metabolic enzymes and mitochondrial and extracellular proteins are slightly underrepresented, whereas known complex members or proteins involved in processes we studied earlier (Hutchins et al., 2010; Maliga et al., 2013) are slightly overrepresented as baits. Membrane proteins are represented according to their fraction in the proteome. (D) Interacting proteins show no biases beyond those of the bait selection and no bias of more than 2-fold. (E) Comparison of annotations of proteins found in the interactome versus never found as interactors showed similar trends. Moreover, it revealed an overrepresentation of nuclear proteins and the term "organelle organization" (which includes cytoskeletal proteins), highlighting the prevalence of protein interactions in these compartments.

(F) 'Hawaii' plot: overlay of all volcano plots of protein enrichments in specific over control IPs plotted against corresponding p values. Two cut-off lines were placed graphically according to the given formula, defining confidence classes A and B. Confidence class C is defined by enrichment > 2 SD without crossing the threshold for classes A or B.

(G) Definition of the cut-off curve parameters x_0 (minimum enrichment) and c (curvature). The point cloud is largely symmetric to the y axis, while meaningful outliers are only expected on the right side (enrichment), but not on the left side (depletion). Any axially symmetric cut-off curve will result in a number of left-sided outliers (false hits) and right-sided outliers (potentially true hits). Conceptually related to the target-decoy approach for peptide and protein identification, the fraction of the left-sided outliers to the total number of outliers serves as an FDR estimate. For a given FDR (shaded areas), a combination of x_0 and c can be selected that maximizes the number of right-sided outliers (red lines). Our cut-offs of 1% and 5% FDR are indicated by dashed lines.

(H) We combined the enrichment FDR with protein profile correlation coefficients across IPs (Keilhauer et al., 2015) to define confidence classes. Classes C and C+ represent cases that did not cross the FDR threshold, but showed enrichments > 2-fold and correlation coefficients > 0.4 and 0.5, respectively. Numbers in brackets represent the numbers of hits for a given confidence class. Note that the number of unique interactions is lower as bait proteins also represent hits and some interactions may be found several times or involving several isoforms.

(I–K) Precision recall curves. For all combinations of the threshold parameters x_0 and c, we calculated precision as estimated by our FDR approach, and recall of interactions in reference datasets, resulting in a precision-recall area (upper panels). The final thresholds of 1% and 5% FDR, respectively (corresponding to 99% and 95% precision) are marked with dashed lines. The lower panels show the total numbers of called interactions, which increases dramatically at high recall. (I) Recall of CORUM-annotated pairs was 49% and 56%, respectively, with most remaining ones clearly behaving as background binders. (J) Recall of CORUM-annotated pairs showing a core stoichiometry signature (see Figure 3B) was substantially higher at 83% and 92%. (K) Recall of interactions with high-confidence reciprocal evidence (< 1% FDR) was 65% and 78%, respectively. All reference datasets show that thresholds are placed as optimal trade-offs in precision-recall space. The reciprocal reference dataset features a more pronounced gain in recall at 5% FDR, emphasizing the benefits of a lower stringent threshold for identifying interactions outside of stable complexes.

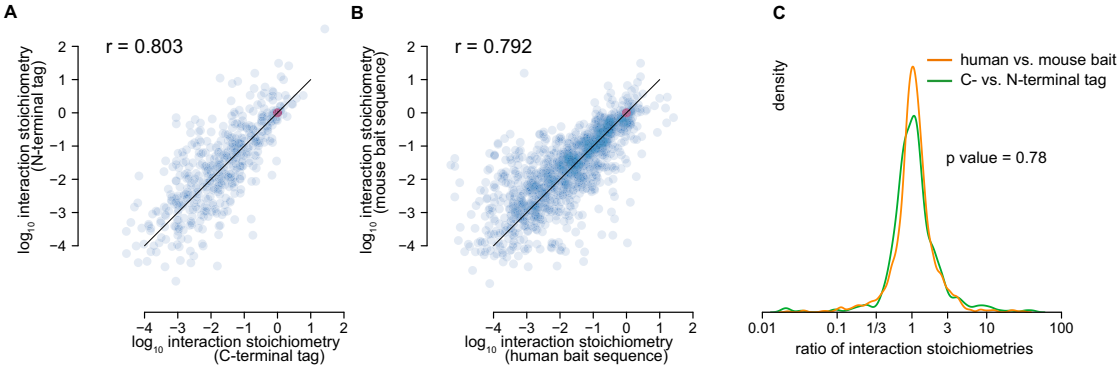

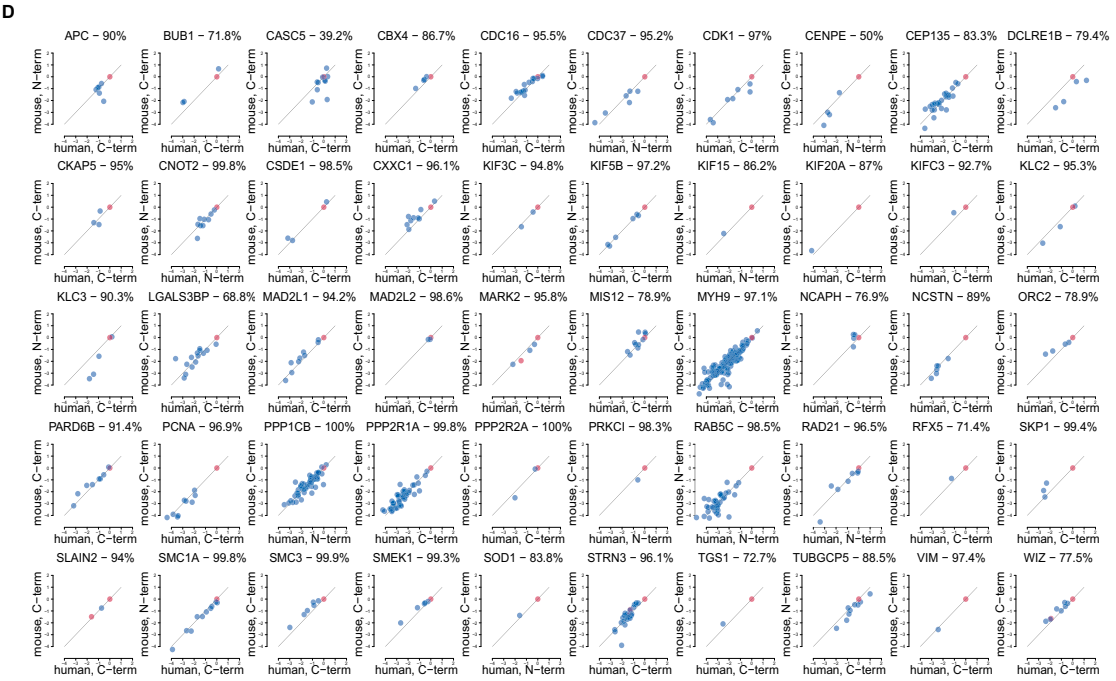

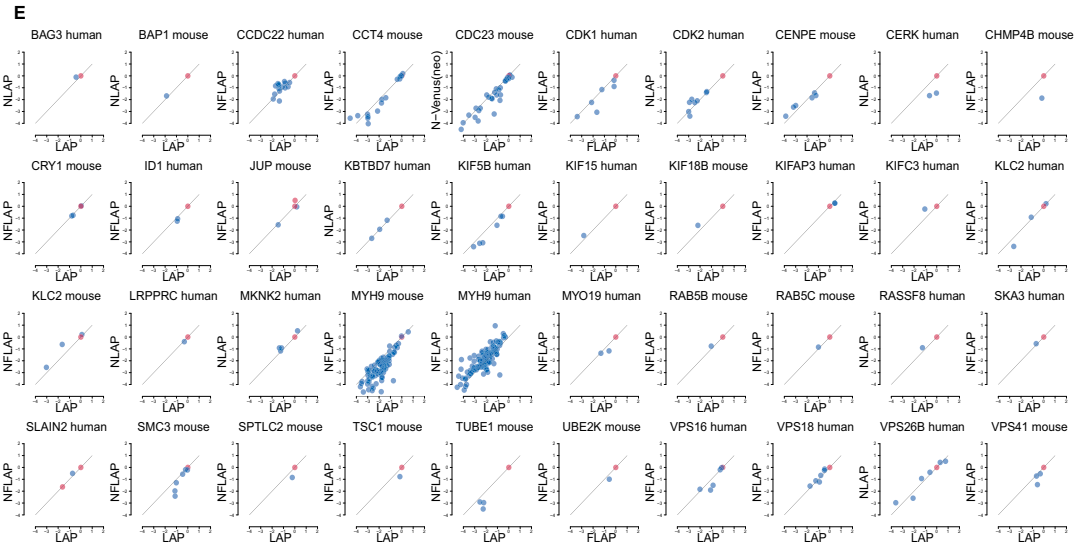

(legend on next page)

Figure S2. Reproducibility of Stoichiometry Values, Related to Figure 2

(A) Correlation of interaction stoichiometry values derived from cell lines using human and mouse ortholog bait sequences (n = 103).

(B) Correlation of interaction stoichiometry values derived from cell lines using N- and C-terminal tags on the same bait sequence (n = 50).

(C) No systematic biases are apparent between human/mouse and N/C-terminal tags and precision of stoichiometries is within a factor of three.

(D) 50 representative examples for mouse versus human.

(E) 40 representative examples for N- versus C-terminal tag.

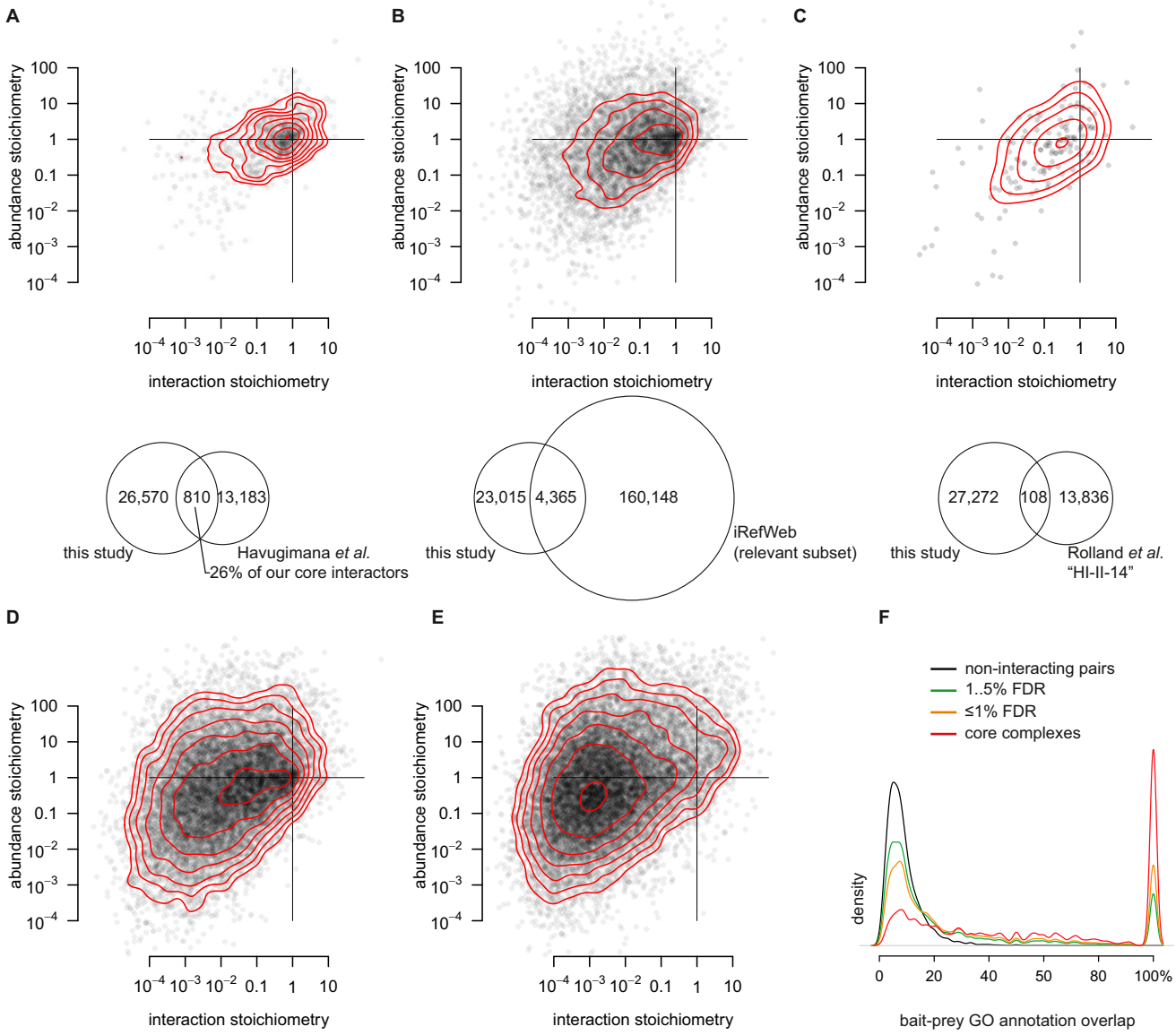

Figure S3. Overlap with Published Datasets, Related to Figure 3

(A) Overlap of our data with published interaction data obtained by protein correlation profiling (Havugimana et al., 2012).

(B) Overlap with relevant interactions in iRefWeb (human; physical; experimental; pairwise or multi-subunit interactions).

(C) Overlap with the "HI-II-14" Y2H dataset (Rolland et al., 2014). Red contour lines separate areas in steps of 1.5-fold increased point density.

(D) Stoichiometry plot of all interactions with FDRs < 1%.

(E) Stoichiometry plot of all interactions with FDRs between 1 and 5%.

(F) Overlap of GO-annotations between pairs of well-annotated proteins (> 3 annotated terms each).

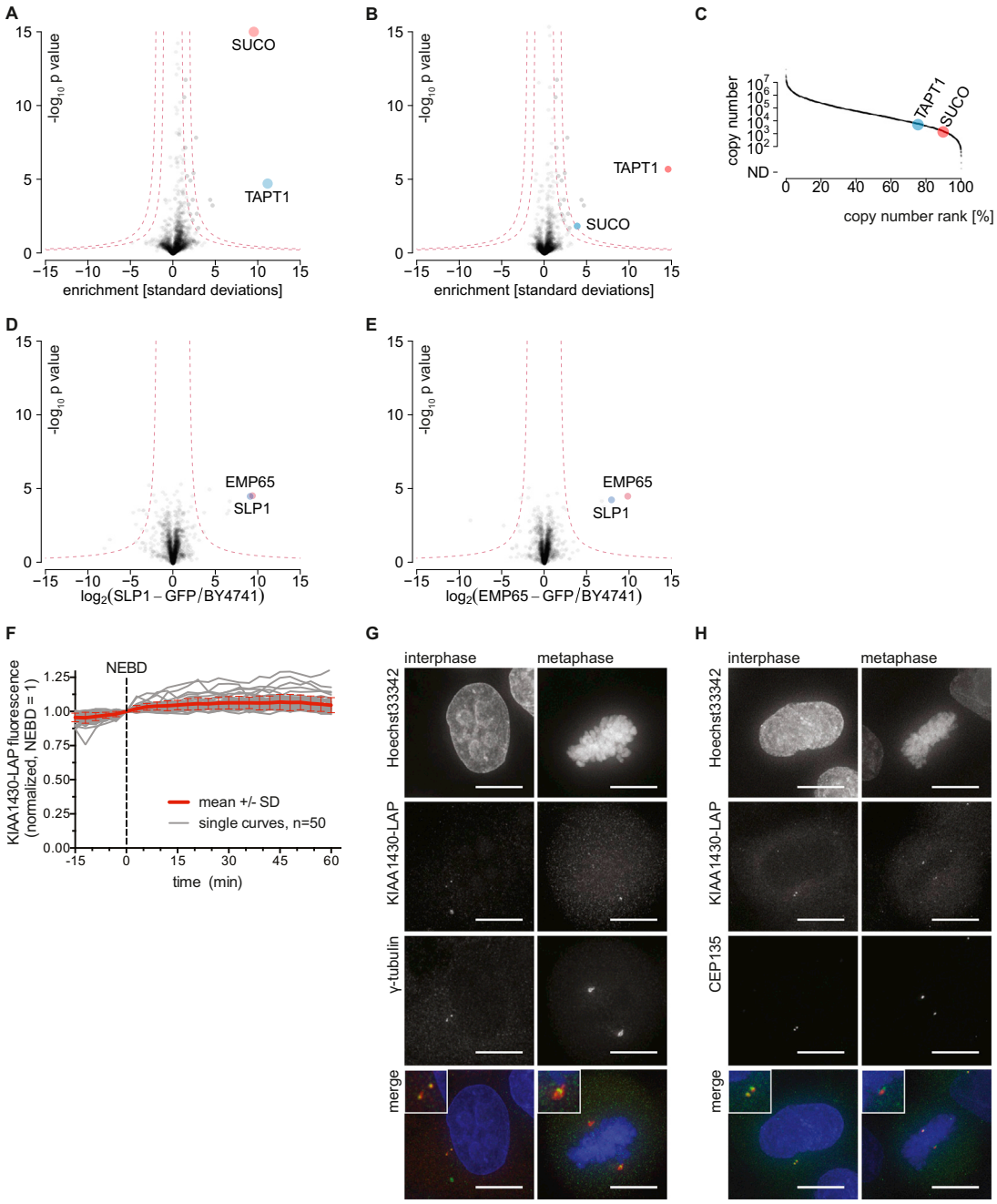

Figure S4. The TAPT1-SUCO Complex and the KIAA1430-APC/C Interaction, Related to Figure 4

(A) Volcano plot of SUCO interactors.

(B) Volcano plot of TAPT1 interactors, providing reciprocal confirmation of the TAPT1-SUCO interaction.

(C) Cellular abundance plot showing copy numbers of TAPT1 and SUCO in the HeLa proteome.

(D) SLP1-GFP pull-down using a strain from the *S. cerevisiae* GFP library (Huh et al., 2003).

(E) EMP65-GFP pull-down. (C) Reciprocal confirmation of the TAPT1-SUCO interaction in HeLa. In all plots, bait proteins are marked in red and relevant interactors in blue.

(F) KIAA1430-LAP fluorescent signal as a function of time before/after nuclear envelope breakdown (NEBD) shows no degradation during mitosis and early G1 phase, indicating that KIAA1430 is not an APC/C substrate.

(G and H) Colocalization of KIAA1430-LAP with the centrosomal marker protein γ-tubulin and the centriolar protein CEP135 in interphase and metaphase. Scale bars, 10 μM.

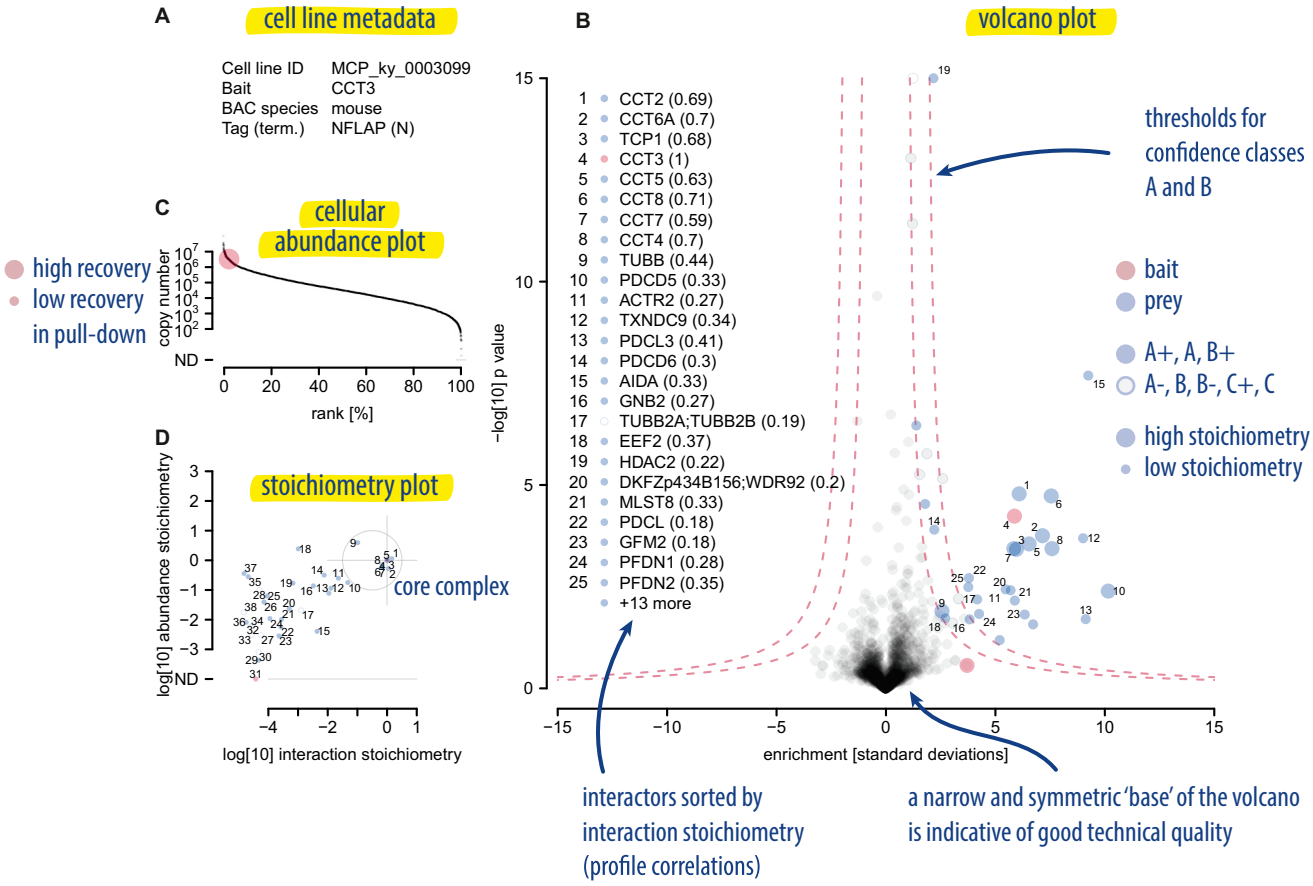

Figure S5. Reading Guide for Data S1, Related to Figure 5

(A) Cell line metadata.

(B) Volcano plot of protein enrichment factors versus negative logarithmized p values as well as threshold lines for different interaction confidence classes.

(C) Cellular abundance plot showing the abundance of the bait in the HeLa proteome.

(D) Stoichiometry plot of interaction and abundance stoichiometries relative to the bait protein.

See also Data S1.

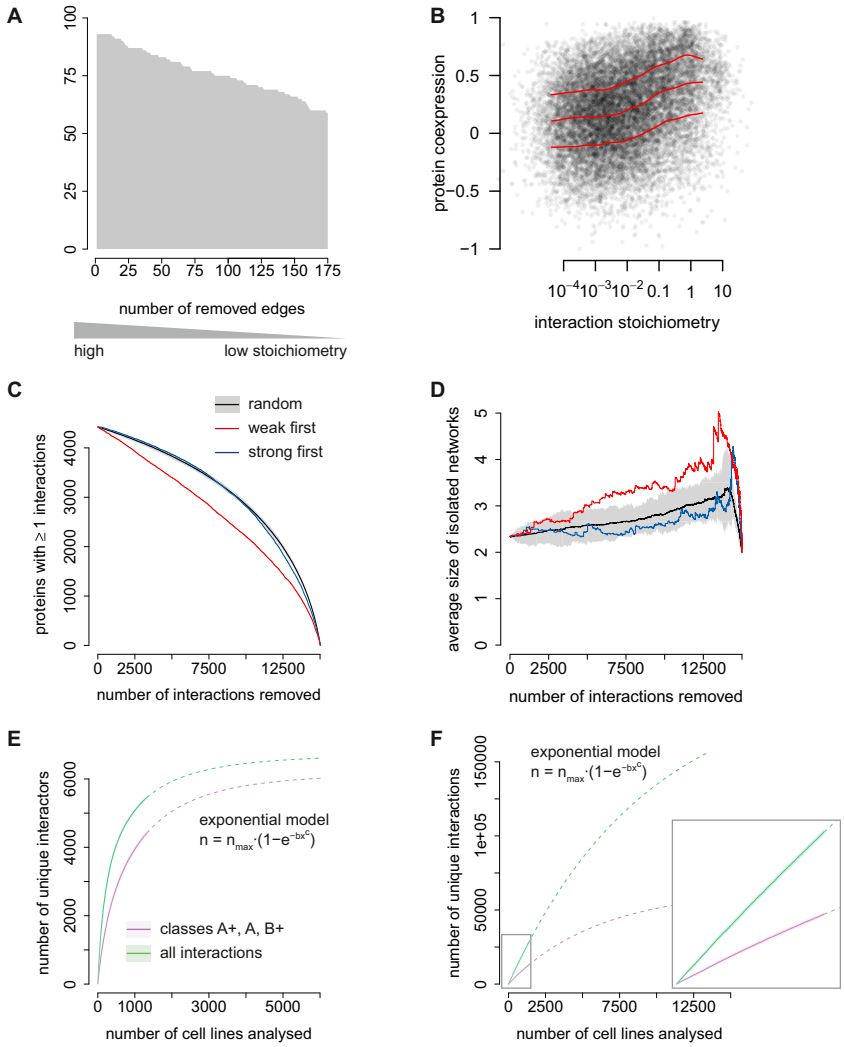

Figure S6. Global Network Properties and Saturation, Related to Figure 6

(A) Preferential removal of strong interactions from the polymerase network causes roughly linear network shrinkage and no fragmentation.

(B) Protein co-expression correlation coefficients (Kim et al., 2014) as a function of interaction stoichiometries.

(C) Effect of the random or targeted removal of interactions on the total number of connected proteins (proteins with $\geq$ 1 interactions).

(D) Effect on the average size of networks isolated from the largest network.

(E) Number of distinct interactors as a function of the number of BAC-GFP line analyzed. Solid lines represent the median of 100 trajectories in randomized order; the scatter indicates the SD from bootstrapping with 100 repetitions. Dashed lines are projections based on a linear model $n = n_{max} \cdot (1 - e^{-bx^c})$ that was fit to the data in the range between cell lines #500 and #1330. The model predicts 6240 and 6420 proteins, respectively, to be coverable.

(F) Number of distinct interactions as a function of the number of BAC-GFP lines analyzed, with projections representing an analogous fit of an exponential model. The model predicts 84,400 and 183,500 as the asymptotic numbers of distinct interactions that can be covered with the highest or with all confidence classes, respectively.

Cell

Supplemental Information

A Human Interactome in Three Quantitative Dimensions Organized by Stoichiometries and Abundances

Marco Y. Hein, Nina C. Hubner, Ina Poser, Jürgen Cox, Nagarjuna Nagaraj, Yusuke Toyoda, Igor A. Gak, Ina Weisswange, Jörg Mansfeld, Frank Buchholz, Anthony A. Hyman, and Matthias Mann

Supplemental Experimental Procedures

Quantitative BAC-GFP interactomics

All interaction experiments were performed using HeLa Kyoto cell lines transformed with bacterial artificial chromosome (BAC) transgenes, which were engineered to introduce an N- or C-terminal tag based on GFP and a functionalized linker sequence (Poser et al., 2008). Such tags are very versatile for both imaging and as affinity handle, and have been used successfully in many studies. While additional affinity tags and protease cleavage sequences are included in some of our tag variants, we exclusively used GFP for affinity enrichment. Differences between the individual tag sequences used are minimal, and mostly relate to additional functionality in the linker or terminal regions. Exact sequences are listed in Table S1 along with metadata and all information regarding our bait collection.

Baits were selected based on availability from earlier studies (Hutchins et al., 2010; Maliga et al., 2013) and the availability of suitable BACs for tagging. We found that the overall collection is devoid of major compositional biases and therefore representative of the cellular proteome (Figure S1C).

For interaction experiments, cells were grown to near-confluency on two 15 cm cell culture dishes per experiment. We harvested three replicates from separate dishes from at least two different culture passages. Cells were detached with accutase (PAA) to limit any unintended general protease activity caused by trypsin, washed and snap frozen.

Pellets were lysed in mild lysis buffer and used as input material for affinity enrichment exactly as described previously (Hubner et al., 2010). In brief, 800 µl of lysate was mixed with magnetic beads pre-coupled to anti-GFP antibodies and run over magnetic microcolumns (Miltenyi Biotec), washed, and subjected to in-column tryptic digestion. Eluates were collected and digestion continued overnight, followed by desalting and storage on StageTips (Ishihama et al., 2006). This was performed in batches of 48 samples on a robotic platform. Replicates of each sample were processed in different batches. MS-analyses were carried out batch-wise, in randomized order within batches, over the course of weeks to months for the replicates of individual samples, preventing any negative influence of column carryover or drifts in machine performance. The entire interaction dataset was recorded using the same dedicated HPLC and Orbitrap instrument.

Label-free quantification and normalization (first dimension of quantification)

MaxQuant's MaxLFQ algorithm calculates a data matrix of label-free quantification (LFQ) intensities that allow the relative comparison of protein amounts across samples with high accuracy (Cox et al., 2014). Additionally, its absolute scaling reflects the summed peptide intensity of a protein or protein group,

which is a measure for the total protein mass. We use the 'match between runs' feature to transfer peptide identifications from MS/MS sequenced peaks to unidentified peaks of the exact same m/z eluting at the same point in the LC gradient in other runs. This leads to a high fraction of valid quantitative data in the data matrix and allows us to gauge the background binding profiles of many proteins. We imputed missing values with random noise simulating the detection limit of the mass spectrometer (Hubner et al., 2010; Eberl et al., 2013; Keilhauer et al., 2015). To this end, imputed values are taken from a log normal distribution with 0.25× the standard deviation of the measured, logarithmized values, down-shifted by 1.8 standard deviations. In this way, we obtained a distribution of quantitative values for each protein across samples. These values represent unspecific binding to the affinity matrix or, in case of imputed values, a simulation of the detection limit of the mass spectrometer.

Interactors are characterized by quantitative enrichment over a negative control, classically a 'mock' sample, for instance a cell line expressing a tag-only construct or the untagged parental cell line. We have shown recently that a cohort of unrelated, tagged cell lines serves as an even better control (Keilhauer et al., 2015). All samples could in principle be used as a control for each individual sample, but it is evident that it is beneficial to exclude related cell lines, such as those where members of the same complex are tagged. Usually, this requires some manual 'flagging' of samples (Jäger et al., 2012; Keilhauer et al., 2015), which becomes impractical with scale. Therefore, we developed a method to exclude those cases in an automated fashion as follows: First, we calculated the median of replicate groups and then the median and interquartile range of the resulting medians. In an iterative fashion, we then removed the most extreme outlier. After that we recalculated the population characteristics. This was repeated until no outlier of more than 1.8 interquartile ranges existed or until 10 groups were removed. The remaining groups of replicates were defined as the control cohort. This procedure proved very effective in determining useful control cohorts without manual intervention, irrespective of the number of samples in the dataset.

Median and standard deviations of the control cohorts represent a robust estimate of background binding behaviour of each protein. We used these values to normalize all quantitative values to represent enrichments in multiples of standard deviations.

Statistical testing, outlier detection and FDR estimation

The control cohort also serves as the reference group for significance testing by a two-sided Welch's *t* test. By plotting the enrichment vs. the negative logarithmized p-values, we obtained "volcano plots", whose name originates from the characteristic shape of the point cloud (Extended Data Fig. 1e).

Most volcano plots have very comparable, narrow distributions of points, which is critical for a reliable determination of a cut-off. A small minority of samples, however, showed rather wide distributions of enrichment factors. We largely found these to be cases of bait proteins co-precipitating the ribosome or

cytoskeletal proteins, both of which contribute the bulk of the background binding protein mass in other pull-downs. In order to apply the same cut-off criteria without including false positives, we implemented a penalty factor that accounts for distortions in the background binding proteome due to specific enrichment of many background binding proteins. The penalty factor is defined in an unbiased way as the intensity-weighted Pearson's correlation coefficient of the averaged protein intensities in each replicate group and the control cohort median. This factor was further divided by the median across all factors and then squared, to be very close to 1.0 for most samples, and <1 in cases with very wide volcano plots. Subsequently, for each cell line, we scaled all enrichment factors by the specific penalty factor. These are listed in Supplementary Table 1.

Outlier detection and FDR estimation

Interactors appear in the upper right corner of the volcano plots and should be separated from the cloud of background binders. A critical parameter for any interaction detection method is the cut-off that separates significant hits from non-significant ones. Several approaches exist to define such a cut-off. Some studies used empirical cut-offs (Collins et al., 2013), while others model distributions of random data and determine the cut-off by the differences between real and simulated data (Sowa et al., 2009; Jäger et al., 2012), or by comparison of literature-derived true positive and false-positive interactions in the dataset (Breitkreutz et al., 2010; Keilhauer et al., 2015).

For volcano plots, cut-offs often involve a minimum fold change and a maximum p-value (Collins et al., 2013). We recently described an approach that uses a graphical formula as a smooth combination of these (Keilhauer et al., 2015):

$$-\log_{10}(p) \geq \frac{c}{|x|-x_0}$$

with

x: enrichment factor of a protein

p: p value of the t test, calculated from replicates

x_0: fixed minimum enrichment

c: curvature parameter.

The curvature parameter c determines the maximum acceptable p value for a given enrichment x.

The parameters c and x_0 can be optimized based on prior knowledge of known true and false positives (Keilhauer et al., 2015).

In this study, we developed a novel approach that relies only on acquired data without the need for gold standards or simulated data. We make use of the fact that a volcano plot of enrichments vs. negative logarithmized p values typically shows a symmetric distribution of points with respect to the y axis. In our

case, this applies to the dominant cloud of background binders. However, there is a marked asymmetry in the outlier populations: while a large number of proteins appear significantly enriched, there were only sporadic cases of proteins apparently being depleted (Extended Data Fig. 1e).

As such 'negative binding' is not expected to occur, this allowed us to define cut-off parameters based on a false discovery rate (FDR) estimation. The proteins beyond the left sided curve are outliers by chance. Therefore we interpret the fraction of left-sided outliers to total outliers as the FDR of calling a point specifically enriched. This concept is borrowed from the target-decoy estimation of peptide identification FDR (Elias and Gygi, 2007), where 1% and 5% are commonly used cut-offs.

For each FDR, different combinations of c and x_0 are possible, and we chose the combination that maximizes the number of right right-sided outliers: 1% FDR: c=3.65 and x_0=1.75; 5% FDR: c=2.9 and x_0=0.9) (Extended Data Fig. 1f).

Interactions with <1% enrichment FDR were assigned to confidence class A, interactions with <5% and >1% to class B.

Profile correlation

Genuinely interacting proteins are often characterized by good correlation of their intensity profiles across samples. Protein correlation profiling is a well-established technique to find stable complexes and to assign proteins to subcellular structures (Andersen et al., 2003; Havugimana et al., 2012; Kristensen et al., 2012). It usually requires extensive fractionation under non-denaturing conditions. In our case, many independent affinity purification experiments serve the same purpose if the proteins are quantified across many samples and we have recently described their use as additional determinants for gauging the significance of statistical outliers (Keilhauer et al., 2015). To this end, we calculate Pearson's correlation coefficients for all candidate interactors. Replicate experiments in which both partners were never quantified (i.e. all values resulted from imputation) were excluded, as they do not contain signal. In the case where one but not the other was quantified, we considered the imputed values. We used the correlation coefficients of interacting proteins as a qualifier in addition to the FDR-controlled confidence classes. Correlation coefficients of 0.1 and 0.2, respectively, correspond to a slight and substantial deviation from the random normal distribution; therefore we chose these values as thresholds for the qualifiers "+" and "–" that we combined with the letters A and B indicating the confidence class.

A small number of interactions showed very high correlation coefficients, in the range of 0.5, while not crossing any FDR threshold. We therefore established the additional confidence classes C and C+ for all interactions with bait enrichments more than two-fold and correlations >0.4 or >0.5, respectively.

Interaction stoichiometries and copy numbers (second/third dimension of quantification)

Comparing the absolute amounts of different proteins by mass spectrometry is inherently more challenging than relative quantification of the same proteins across samples. This is because the peak intensities of different peptides depend not only on their amounts, but also on the ionization efficiencies of the peptide. Available methods therefore often employ isotopically labelled spike-in references of known quantities. Combining the known amount of the spike-in with relative quantification readout yields the stoichiometries of individual proteins in the sample. Clearly, labelled spike-ins are not practicable in a dataset of our scale, as this approach would require prior knowledge of which proteins are to be quantified.

However, label-free approaches of absolute quantification are viable alternatives and provide useful estimates that can be used to gauge stoichiometries. Available methods seek to circumvent or normalize the different properties of individual peptides by taking only the sum of the top three 'best flying' peptides (Malmstrom et al., 2009) or dividing the summed intensities of all peptides by the size of the protein or the number of theoretical peptides (Schwanhäusser et al., 2011; Wisniewski et al., 2014). We normalized our LFQ intensities – label-free signals as extracted and calculated by the MaxQuant software's MaxLFQ module (Cox et al., 2014) – by the number of theoretical tryptic peptides between 7 and 30 amino acids in length for any given protein, which is the approach taken in the iBAQ method (Schwanhäusser et al., 2011). This allows the estimation of relative molar amounts of different proteins in a sample.

To calculate interaction stoichiometries, we subtracted the background binding intensities (see section 1) to account for the amounts of the proteins bound unspecifically, before reporting the ratio of each prey normalized to the bait. A similar approach was recently validated and applied to a number of chromatin-associated protein complexes, with a reported accuracy that allowed the estimation of how many copies of each subunit made up the complexes (Smits et al., 2012).

In a similar fashion, one can estimate the relative abundances of proteins in whole proteome samples. By scaling these values to the total amount of protein per cell, we obtained copy numbers of each protein (Wisniewski et al., 2012; Wisniewski et al., 2014). Specifically, we set the sum of all copy numbers multiplied by the respective molar masses as equal to 200 pg in a cell volume of 1 pl.

Conversely, a typical IP sample contains around 1-3 µg of peptides, so we set 1 µg or 25 pmol of an average protein as the equivalent of the typical cumulative intensity of all background binders and thereby estimated the absolute amount of each bait protein recovered after IP.

PAM-SILAC dynamic interactor exchange experiments

Tagged and parental HeLa lines were metabolically labeled with $^{13}C_6{}^{15}N_4$-arginine and $^{13}C_6{}^{15}N_2$-lysine, or their light counterparts, for 2 weeks in media containing dialyzed serum. Cells were lysed using the standard lysis conditions. Heavy, tagged and light, untagged lysates (and vice versa) were mixed 1:1 to a total volume of 800 µl immediately before subjecting them to the standard affinity enrichment protocol. The incubation time for dynamic exchange was 15 minutes. Each cell line was analyzed with label-swap and in triplicate for each labeling state. Raw files were processed in MaxQuant with the 're-quantify' feature activated and requiring 1 minimum ratio count.

APC/C–KIAA1430 experiments

For APC3 immunoprecipitations, HeLa Kyoto cell lines expressing KIAA1430-LAP were arrested in mitosis with 330 nM nocodazole (Sigma) using a double thymidine block and release protocol, immunoprecipitated using a specific antibody (clone AF3.1, gift from T. Hunt, CRUK, London, UK), followed by elution of bound proteins with 1 mg/ml of competing peptide, and western blot detection (Mansfeld et al., 2011). To analyze the effect of KIAA1430 depletion, cells were transfected with 70 nM esiRNA (Eupheria Biotech) and after 72 h treated with 0.5 µM reversine (Biomol) as indicated and analyzed by time-lapse imaging. To monitor KIAA1430-LAP localization during the cell cycle iRFP was targeted into the histone 3.1 locus as described (Collin et al., 2013). KIAA1430-LAP stability and co-localization with centrosomes was analyzed by time-lapse imaging and immunostaining against γ-tubulin (Sigma) and CEP135 (Abcam), respectively.

Supplemental Tables

Table S4. Proteins co-enriched with GFP-tagged TRiC subunits.

Related to Figure 5.

Listed are all prey proteins that scored as interactors in at least two sets of TRiC pull-downs. Numeric values represent medians of all evidences.

Prey	Type	Correlation	# of times found	log10 interaction stoichiometry	log10 abundance stoichiometry
CCT2	TRiC core	0.754	6	0.173	0.176
CCT6A		0.772	6	0.020	-0.135
TCP1		0.682	6	0.011	0.154
CCT5		0.789	6	-0.030	0.047
CCT4		0.798	6	-0.083	0.000
CCT3		0.744	6	-0.112	0.131
CCT7		0.759	6	-0.207	-0.139
CCT8		0.774	6	-0.225	-0.112
PDCD5	regulatory protein	0.414	6	-1.606	-0.641
TXNDC9		0.401	6	-1.683	-0.856
PDCL3		0.472	6	-1.953	-0.987
PDCL		0.357	6	-3.162	-2.098
FAM203A/B		0.242	6	-3.727	-1.257
PFDN1	co-chaperon	0.228	2	-3.879	-1.924
PFDN2		0.378	2	-4.094	-1.120
TUBB	cyto-skeleton	0.408	4	-0.732	0.721
TUBA1B		0.426	2	-1.177	0.658
ACTR2		0.281	6	-2.067	-0.514
ACTR1A		0.170	2	-2.256	-0.499
ACTL8		0.124	4	-3.709	-2.157
GNB2	WD domain protein	0.145	4	-2.904	-0.818
EIF3I		0.236	4	-3.421	-0.412
MLST8		0.303	4	-3.691	-1.954
WDR92		0.375	5	-3.753	-1.531
CSTF1		0.245	3	-3.866	-0.788
WDR77		0.097	3	-4.119	-0.860
RFWD3		0.299	2	-4.315	-2.766
DTL		0.223	3	-4.578	-2.951
RPTOR		0.206	2	-4.666	-2.764
PPP6C	phosphatases	0.376	2	-3.052	-1.131
IGBP1		0.236	2	-3.337	-1.412
ESCO1	other	0.089	2	-2.843	-3.577
CCDC47		0.055	2	-3.615	-1.004
TNPO1		0.188	2	-4.683	-0.335

Table S5. Proteins co-enriching TRiC. Related to Figure 5.

Listed are all bait proteins in whose pull-downs at least three TRiC core subunits were scored as interactors. Numeric values represent medians of all TRiC subunit values.

Bait	Type	Correlation	# of TRiC subunits	log10 interaction stoichiometry	log10 abundance stoichiometry
CCT7	TRiC core	0.788	8	0.243	0.166
CCT4		0.720	8	-0.002	0.020
CCT3		0.692	8	-0.005	-0.084
CCT8		0.813	8	-0.025	0.142
CCT4		0.790	8	-0.059	0.027
CCT2		0.742	8	-0.149	-0.115
TUBA3C/E	cyto-skeleton	0.233	8	0.190	NA
TUBA3C/E		0.226	8	-0.181	NA
TUBG1		0.310	8	-0.609	0.836
TUBG1		0.310	8	-0.733	0.836
TUBG1		0.310	8	-0.873	0.836
TUBG1		0.185	8	-0.934	0.855
TUBA1C		0.371	8	-1.759	-0.577
TUBE1		0.081	6	-2.193	2.121
ACTR1B		0.099	7	-2.636	2.218
TUBE1		0.096	3	-2.912	2.226
ACTB		0.084	4	-3.585	-0.880
ACTR2		0.285	8	-1.843	0.583
PPP4C	phospha-tases	0.173	8	0.074	1.275
PPP2CB		0.280	8	-0.794	0.437
PPP2CA		0.133	8	-0.822	0.315
PPP2CA		0.182	8	-0.906	0.323
PPP6C		0.362	8	-1.012	1.230
IGBP1		0.274	8	-1.406	1.378
WDR61	WD domain protein	0.103	8	1.085	0.675
WDR48		0.106	8	0.010	1.414
GNB1		0.244	8	-0.248	0.679
RFWD3		0.155	8	-0.308	2.650
NSMAF		0.194	8	-0.361	2.513
DDB2		0.129	8	-0.866	1.552
STRN3		0.258	8	-1.486	1.740
DTL		0.103	8	-1.501	3.123
STRN3		0.258	8	-1.522	1.740
NEDD1		0.119	8	-1.930	2.142
KIF21B		0.114	7	-2.090	2.929
KIF21A		0.047	8	-2.109	1.566
WRAP53		0.056	8	-2.156	1.717
CDC20		0.203	7	-2.222	2.013
STRN		0.322	8	-2.224	1.345
PRPF4		0.138	8	-2.473	1.106
SEH1L		0.107	4	-2.792	1.028
NEDD1		0.413	8	-2.656	2.098
NEDD1		0.413	8	-1.053	2.098
BUB3		0.105	3	-3.766	1.026
SAMM50	other	0.134	8	-0.401	1.288
NIPSNAP1		0.136	8	-0.832	1.172
PDK3		0.140	8	-1.022	2.989
HDAC1		0.182	8	-1.276	0.614
ARMC6		0.144	8	-1.647	1.622
JAK3		0.103	4	-1.941	4.128
XRCC3		-0.009	4	-2.331	3.967
ILK		0.107	7	-2.636	1.545
CDK1		0.219	4	-3.655	0.337

Supplemental References

Andersen, J.S., Wilkinson, C.J., Mayor, T., Mortensen, P., Nigg, E.A., and Mann, M. (2003). Proteomic characterization of the human centrosome by protein correlation profiling. Nature *426*, 570-574.

Breitkreutz, A., Choi, H., Sharom, J.R., Boucher, L., Neduva, V., Larsen, B., Lin, Z.Y., Breitkreutz, B.J., Stark, C., Liu, G., *et al.* (2010). A global protein kinase and phosphatase interaction network in yeast. Science *328*, 1043-1046.

Collin, P., Nashchekina, O., Walker, R., and Pines, J. (2013). The spindle assembly checkpoint works like a rheostat rather than a toggle switch. Nat Cell Biol *15*, 1378-1385.

Collins, B.C., Gillet, L.C., Rosenberger, G., Rost, H.L., Vichalkovski, A., Gstaiger, M., and Aebersold, R. (2013). Quantifying protein interaction dynamics by SWATH mass spectrometry: application to the 14-3-3 system. Nat Methods *10*, 1246-1253.

Cox, J., Hein, M.Y., Luber, C.A., Paron, I., Nagaraj, N., and Mann, M. (2014). Accurate Proteome-wide Label-free Quantification by Delayed Normalization and Maximal Peptide Ratio Extraction, Termed MaxLFQ. Mol Cell Proteomics *13*, 2513-2526.

Eberl, H.C., Spruijt, C.G., Kelstrup, C.D., Vermeulen, M., and Mann, M. (2013). A map of general and specialized chromatin readers in mouse tissues generated by label-free interaction proteomics. Mol Cell *49*, 368-378.

Elias, J.E., and Gygi, S.P. (2007). Target-decoy search strategy for increased confidence in large-scale protein identifications by mass spectrometry. Nat Methods *4*, 207-214.

Havugimana, P.C., Hart, G.T., Nepusz, T., Yang, H., Turinsky, A.L., Li, Z., Wang, P.I., Boutz, D.R., Fong, V., Phanse, S., *et al.* (2012). A census of human soluble protein complexes. Cell *150*, 1068-1081.

Hubner, N.C., Bird, A.W., Cox, J., Splettstoesser, B., Bandilla, P., Poser, I., Hyman, A., and Mann, M. (2010). Quantitative proteomics combined with BAC TransgeneOmics reveals in vivo protein interactions. J Cell Biol *189*, 739-754.

Hutchins, J.R., Toyoda, Y., Hegemann, B., Poser, I., Heriche, J.K., Sykora, M.M., Augsburg, M., Hudecz, O., Buschhorn, B.A., Bulkescher, J., *et al.* (2010). Systematic analysis of human protein complexes identifies chromosome segregation proteins. Science *328*, 593-599.

Ishihama, Y., Rappsilber, J., and Mann, M. (2006). Modular stop and go extraction tips with stacked disks for parallel and multidimensional Peptide fractionation in proteomics. Journal of proteome research *5*, 988-994.

Jäger, S., Cimermancic, P., Gulbahce, N., Johnson, J.R., McGovern, K.E., Clarke, S.C., Shales, M., Mercenne, G., Pache, L., Li, K., *et al.* (2012). Global landscape of HIV-human protein complexes. Nature *481*, 365-370.

Keilhauer, E.C., Hein, M.Y., and Mann, M. (2015). Accurate protein complex retrieval by affinity enrichment mass spectrometry (AE-MS) rather than affinity purification mass spectrometry (AP-MS). Mol Cell Proteomics *14*, 120-135.

Kristensen, A.R., Gsponer, J., and Foster, L.J. (2012). A high-throughput approach for measuring temporal changes in the interactome. Nat Methods *9*, 907-909.

Maliga, Z., Junqueira, M., Toyoda, Y., Ettinger, A., Mora-Bermudez, F., Klemm, R.W., Vasilj, A., Guhr, E., Ibarlucea-Benitez, I., Poser, I., *et al.* (2013). A genomic toolkit to investigate kinesin and myosin motor function in cells. Nat Cell Biol *15*, 325-334.

Malmstrom, J., Beck, M., Schmidt, A., Lange, V., Deutsch, E.W., and Aebersold, R. (2009). Proteome-wide cellular protein concentrations of the human pathogen Leptospira interrogans. Nature *460*, 762-765.

Mansfeld, J., Collin, P., Collins, M.O., Choudhary, J.S., and Pines, J. (2011). APC15 drives the turnover of MCC-CDC20 to make the spindle assembly checkpoint responsive to kinetochore attachment. Nat Cell Biol *13*, 1234-1243.

Poser, I., Sarov, M., Hutchins, J.R., Heriche, J.K., Toyoda, Y., Pozniakovsky, A., Weigl, D., Nitzsche, A., Hegemann, B., Bird, A.W., *et al.* (2008). BAC TransgeneOmics: a high-throughput method for exploration of protein function in mammals. Nat Methods *5*, 409-415.

Schwanhäusser, B., Busse, D., Li, N., Dittmar, G., Schuchhardt, J., Wolf, J., Chen, W., and Selbach, M. (2011). Global quantification of mammalian gene expression control. Nature *473*, 337-342.
Smits, A.H., Jansen, P.W., Poser, I., Hyman, A.A., and Vermeulen, M. (2012). Stoichiometry of chromatin-associated protein complexes revealed by label-free quantitative mass spectrometry-based proteomics. Nucleic Acids Res.
Sowa, M.E., Bennett, E.J., Gygi, S.P., and Harper, J.W. (2009). Defining the human deubiquitinating enzyme interaction landscape. Cell *138*, 389-403.
Wisniewski, J.R., Hein, M.Y., Cox, J., and Mann, M. (2014). A 'proteomic ruler' for protein copy number and concentration estimation without spike-in standards. Mol Cell Proteomics.
Wisniewski, J.R., Ostasiewicz, P., Dus, K., Zielinska, D.F., Gnad, F., and Mann, M. (2012). Extensive quantitative remodeling of the proteome between normal colon tissue and adenocarcinoma. Mol Syst Biol *8*, 611.